6. Proposed Modifications to Achieve EPU Target Stress Levels

The dryer analyzed in the previous section contains several locations with alternating stress ratios below the EPU target 2.00. As described above in Section 3.1 the dryer already contains several planned reinforcements previously identified to meet target stresses when using the ACM Rev. 4.0 acoustic loads predictions with noise left in [5]. Because of changes in dominant frequency peaks and the generally more conservative loads model (limited filtering, no noise subtraction, etc.) additional reinforcements are now necessary. To meet the requested EPU stress margins modification are required and the present section is concerned with proposing and analyzing these modifications.

To this end the locations whose alternating stress ratios fall below target values in Table 9b are grouped into distinct sets in Table 10. There are four main groups:

Group 1: The lifting rod bracket/side plate welds. The upper and middle brackets already have weld reinforcement, but this does not reduce stresses sufficiently under the new loads.
Group 2: The middle hood reinforcement strip incurs a high stress due to vibration of the outboard section of the middle hood.
Group 3: The inner hood/hood support welds that experience high stresses due to the inner hood vibrations.
Group 4: The remaining points which are readily modified to achieve SR-a>2.76 as discussed further below.

For reference, the two final columns in Table 10 record: (i) The limiting alternating stress ratio using the stress allowable of 16.5 ksi obtained from curve B of Fig. I-9.2.2 in Appendix I of Section III in the ASME B&PV Code; when this allowable is used all of the locations in Group 4 meet margin and only four of the locations in the table require modification. (ii) The estimated stress ratio after implementing the recommended modifications developed below (for this last column the more conservative stress allowable of 13.6 ksi inferred from curve C is used).

Below, these groups are discussed in further detail.

Table 10. List of locations from Table 9b with alternating stress ratios below 2.76 re-ordered into groups.

Location	GROUP	SRF	node	Pm	Pm+Pb	Sa	SR-P	SR-a	% Freq. Shift	Dom. Freq. [Hz]	SR-a Curve B(c)	SR-a Post Mod.(d)
1. Side Plate/Brace	1	0.6(5)	89649	4022	5464	4413	2.31	1.56	-5	139.7	1.89	5.20 (Concept 2)
3. Side Plate/Brace	1	1	89646	3460	4435	3947	2.69	1.74	5	103.3	2.11	5.80 (")
7. Side Plate/Brace	1	0.6(5)	89652	2656	3752	2924	3.5	2.35	-5	139.7	2.85	7.83 (")
2. Hood Reinforcement/Middle Hood	2	1	98275	414	4626	4229	3.01	1.62	10	109.0	1.97	34.3
8. Hood Reinforcement/Middle Hood	2	1	90126	1090	3925	2918	3.55	2.35	10	109.0	2.85	33.1
9. Hood Reinforcement/Middle Hood	2	1	98268	665	2992	2889	4.66	2.38	-7.5	146.1	2.89	28.6
10. Hood Reinforcement/Middle Hood	2	1	90949	1071	2776	2673	5.02	2.57	2.5	190.7	3.12	22.6
4. Hood Support/Inner Hood	3	1(b)	95636	1160	3228	3172	4.32	2.17	-10	51.2	2.63	3.29
5. Hood Support/Inner Hood	3	1(b)	95650	1126	3277	3027	4.25	2.27	-10	51.2	2.75	4.18
6. Hood Support/Inner Hood	3	1(b)	95642	1270	3023	3017	4.61	2.28	2.5	44.1	2.77	3.05
11. Hood Support/Outer Base Plate/Middle Backing Bar	4	1(b)	95428	4516	4994	2593	2.06	2.65	5	48.6	3.22	4.08 (stress relief notch)
14. Hood Support/Outer Cover Plate/Outer Hood	4	1(b)	95267	4892	5223	2538	1.9	2.71	-10	60.5	3.29	4.17 (stress relief notch)
12. Submerged Drain Channel/Submerged Skirt	4	1	93430	820	6224	2591	2.24	2.65	5	51.8	3.22	4.57 (SRF=0.58)
15. Submerged Drain Channel/Submerged Skirt	4	1	84597	1167	4640	2527	3	2.72	2.5	104.0	3.30	4.69 (")
13. Hood Support/Middle Hood	4	1(b)	96022	905	2750	2562	5.07	2.68	-5	53.4	3.25	>2.76 est. (add mass)

Notes.

(a) Node numbers are retained for further reference.

(1-8) Appropriate stress reduction factor for the welds and modifications listed in Table 7 have been applied. The number refers to the particular location and corresponding stress reduction factor in Table 7.

(b) WF=1.4

(c) Stress ratio calculated on the basis of curve B (16.5 ksi allowable) of Fig. I-9.2.2 in Appendix I of Section III in the ASME B&PV Code.

(d) Estimated stress ratio after modifications outlined below (using Curve C with the 13.6 ksi allowable).

Lifting Rod Support Brackets (Group 1)

The limiting alternating stress locations occur on the lifting rod support brackets (SR-a=1.56). A stress reduction factor of 0.6 is already imposed on the upper and next lower brackets to account for a planned reinforcement of the existing weld. The stresses are highly localized (only one node on each such bracket is affected) which is indicative of development of stress singularities at this re-entrant corner. The dominant frequencies for these locations are found to lie about the 98 Hz (for the lowest bracket) and 130-140 Hz (middle and upper brackets) frequency ranges. If the lower brackets are modified using the same weld reinforcement planned for the middle and upper brackets then their limiting alternating stress ratio increases to 2.90. However, the middle and upper brackets are still below target stress ratios and further weld reinforcement appears unlikely by itself to achieve the necessary stress reductions. Instead a more substantial structural reinforcement is required.

For the limiting node (89649) on the upper support bracket the signal frequency producing the largest stress contribution occurs at 139.7 Hz. Since this signal is shifted -5%, it excites a structural response at 132.7 Hz. The structural response in the vicinity of this frequency is examined further by identifying how the unit solution stress intensity at this node varies over the 90-150 Hz frequency range. Figure 18 records this stress intensity for each of the four unit solutions (recall that a unit solution is developed by setting the pressure to unity at one MSL and zero at the others). The dominant peak in the unit solutions occurs at 136.6 Hz. Figure 19 records the unit solution displacement and stress responses at this frequency and shows the lifting rod vibrating in a restrained (by the brackets) second order mode. The localized stress concentrations on the re-entrant corners of the support brackets are clearly apparent in the lower plot in Figure 19.

In order to reduce stresses and meet target EPU stress ratios the model was modified by increasing the thickness of all elements adjacent to the weld line from 0.375" to 0.75". This includes elements from the end plate as well as the brace. The collection of modified elements is shown in Figure 20. Unit solutions were then recomputed for the modified model and compared to those obtained without modification. Figure 21 compares the steam dryer responses of the modified and unmodified brackets at the limiting frequency, 136.6 Hz. In general the high stresses are reduced by approximately an order of magnitude over the entire frequency range considered. Away from the high stress locations the structural response is virtually unchanged. This is expected since the high stress and remedial reinforcements are highly localized so that the modal properties are left unaltered.

On the basis of these results the reinforcement concepts proposed for the lifting rod support bracket (Figure 22) are outlined in Figure 23. The first, and most conservative, concept Figure 23a) effectively thickens the bracket to ¾" by overlaying a strip parallel to the weld line as indicated. In addition a 3/8" thick rounded rectangular plate is placed on the side plate as shown. This concept would require severing and grinding clear the existing weld connecting the bracket to the side plate, welding the two plates to the respective components and re-welding the bracket back in place. The second concept Figure 23b) is less invasive and reinforces only the region about the high stress point. It involves the insertion and weld attachment of a semi-circular 2" radius disc on the end-plate as indicated. This requires removal of the existing weld in the vicinity of the high stress spot. In addition a small reinforcement plate, shaped to match the re-entrant corner contour as shown, is welded onto the support bracket to increase the effective thickness and thereby reduce the membrane stress. The third concept Figure 23c) is similar to the preceding one, but without the semi-circular disc and increases the overall size of the contour-matching plate welded onto the support bracket. This third concept takes advantage of the observation (see, for example, Figure 18) that the maximum stress is a membrane stress that

occurs in the bracket; the alternating stresses in the side plate are comparatively low. It also is least intrusive in that weld removal is kept to a minimum. The final concept (Figure 23d) is derived from concept 2 by retaining the 2" circular disk on the side plate, but discarding the brace reinforcement. The last three concepts require that the remaining bracket/side plate weld still be increased to ½". This is necessary to ensure that stresses at the weld end opposite to the one being addressed here remain below target levels.

A quantitative assessment of these concepts is performed by evaluating the maximum stress reduction in the unit solution stresses over the 128–145 Hz frequency range which brackets the dominant frequencies for this location in the global solution. The concepts are modeled by selectively increasing the local thickness. For the full modification concept 1, all elements with at least one node on the lifting rod brace/side plate connection are thickened from 0.375 to 0.75. For the partial modification concept 2, only elements with a node on the single high stress location are thickened. For concept 3 (brace reinforcement) only those elements from concept 2 that lie on the brace are reinforce. Conversely for concept 4 (side plate reinforcement) only those elements from concept 2 that lie on the side plate have increased thickness. The results from these concepts are summarized in Table 11 which records the limiting stress over the 128–145 Hz frequency range at each of the listed nodes. The nodes are identified from the global solution as being the most limiting at CLTP in the baseline dryer configuration (without these modifications). The limiting nodal stress is taken as the maximum of all unit solution stresses at this node over the afore-stated frequency range. The maximum stress for all five nodes is also listed together with the reduction in this maximum stress for each of the proposed concepts. Not surprisingly, the full reinforcement of the brace and side plate produces the greatest reduction in maximum stresses as reflected in the reduction factor of 0.14. All of the other concepts also produce reductions. Interestingly the side plate reinforcement (concept 4) is more effective at reducing stresses than the brace reinforcement (concept 3) despite the observation that the maximum stresses occur in the brace. A stress reduction by a factor of 0.34 is required to bring the CLTP stresses to 2.76. Using the reduction factors Table 11 then all of the proposed concepts except concept 3 bring the stresses to within the target stress levels.

Selecting the optimal concept (i.e., the one achieving the necessary stress reduction with minimal weld removal) will proceed on the basis of additional structural evaluation and cost-benefit analysis. For the lower-most brackets the required stress margin can either be met by implementing the same concept selected above for the middle and upper brackets or by simply reinforcing the existing bracket/side plate weld to ½" which has already been shown to provide sufficient stress reduction for these brackets.

Table 11. Group 1 unit solution stresses using various proposed reinforcement concepts

Node	No Mods.	Limiting Nodal Stress [psi]			
		Full Mod (Concept 1)	Partial mod. (Concept 2)	Brace Mod (Concept 3)	Side Plate Mod (Concept 4)
89649	30439	4138	5098	17118	8690
87627	30348	4131	5001	17398	7978
103160	28247	4169	5297	15910	8458
90307	30205	4018	5316	16852	8921
89652	14163	2999	4345	8788	7069
Max. Stress	**30439**	**4169**	**5316**	**17398**	**8921**
Reduction in Max. Stress	N/A	**0.14**	**0.18**	**0.57**	**0.29**

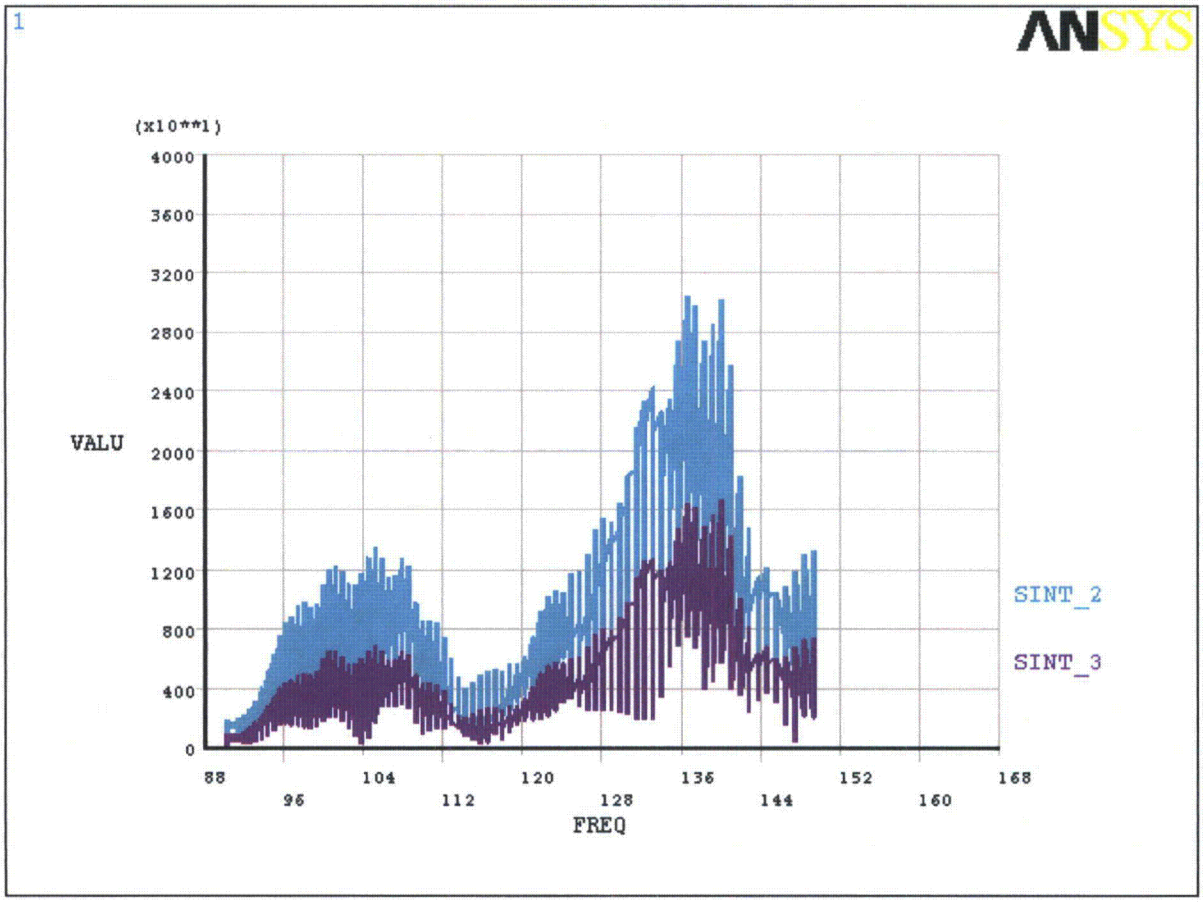

Figure 18. Variation of stress intensity with frequency at high stress location (node 89649) on lifting support brace with no modifications. Results for all steam line unit solutions are plotted at each frequency. SINT_2 is the stress in the brace and SINT_3 is the stress in the side plate

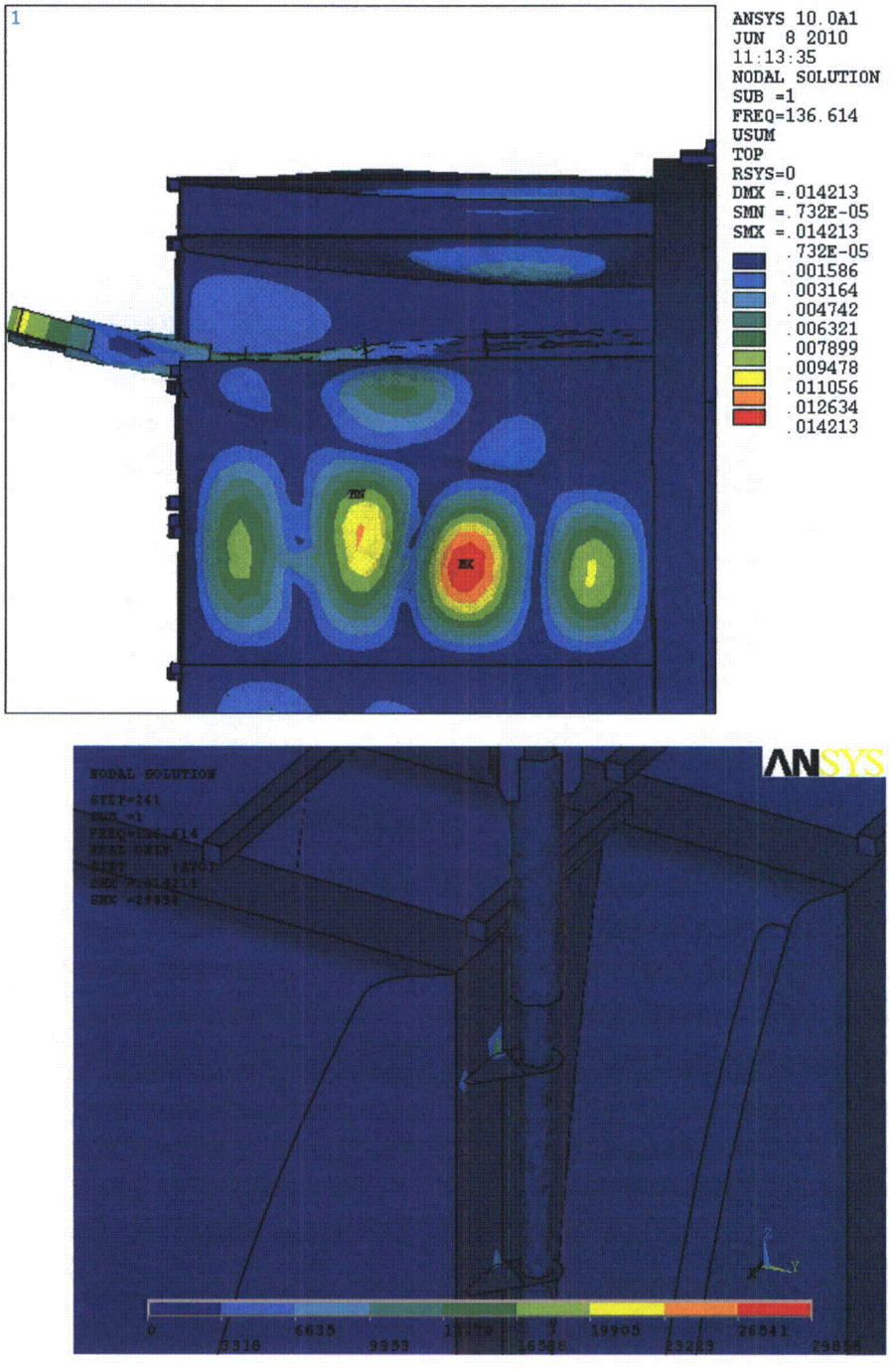

Figure 19. Unit solution at 136.6 Hz. Top – displacements, bottom – stresses. Bottom model is rotated to show high stress locations on the side plates.

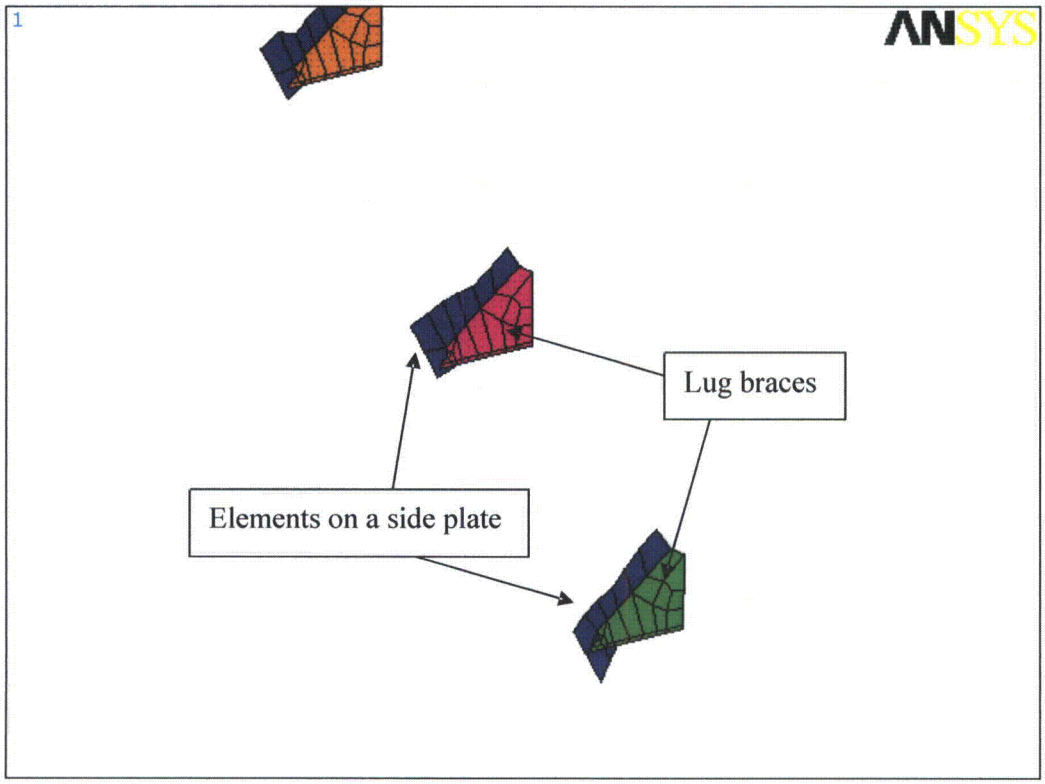

Figure 20. The elements adjacent to the lifting rod bracket/side plate weld whose thicknesses are increased from 0.375" to 0.75".

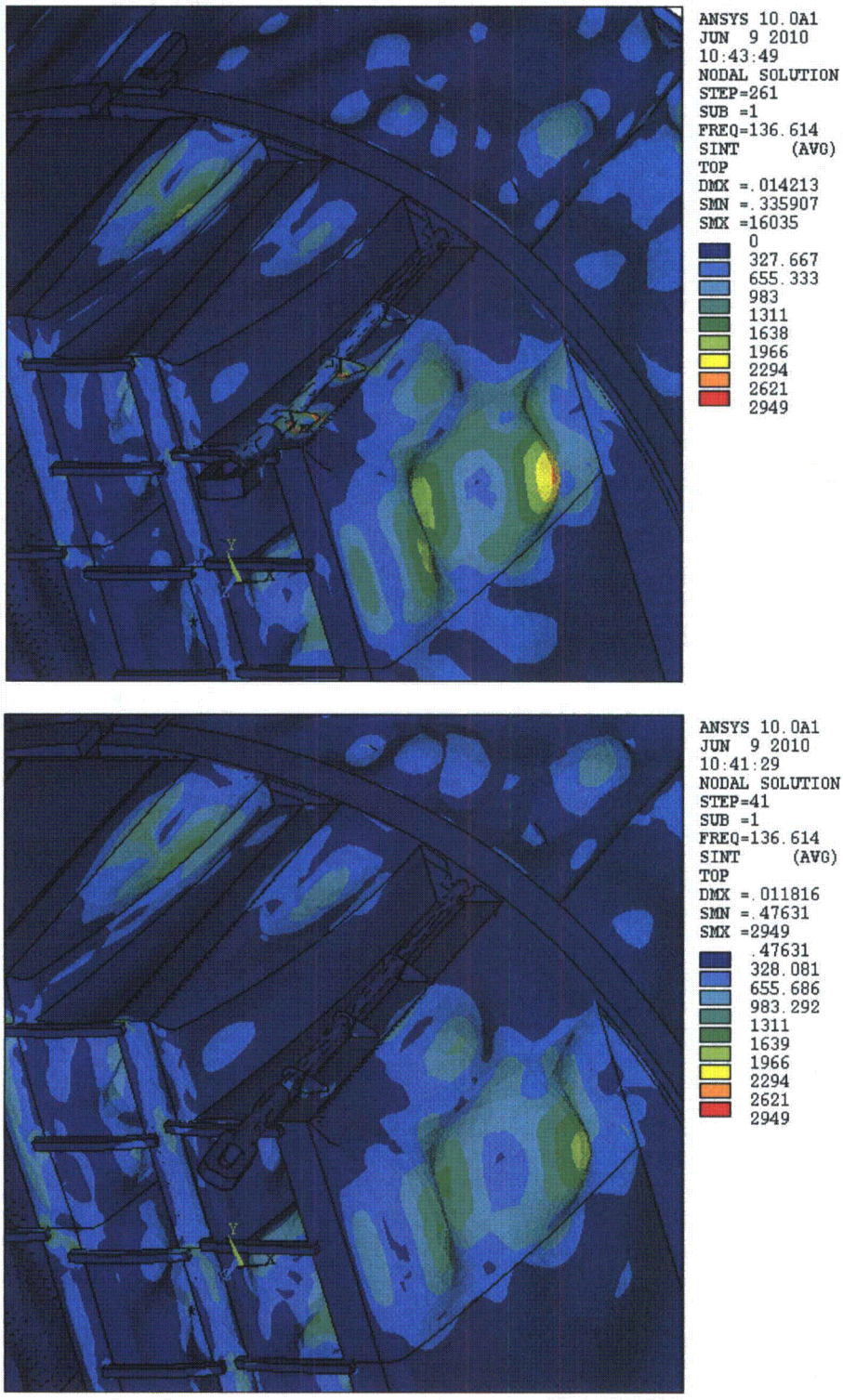

Figure 21. Structural response at 136.6 Hz. Top – no modification to lifting rod braces. Bottom –lifting rod brackets and side plate elements adjacent to weld thickened from 3/8" to 3/4".

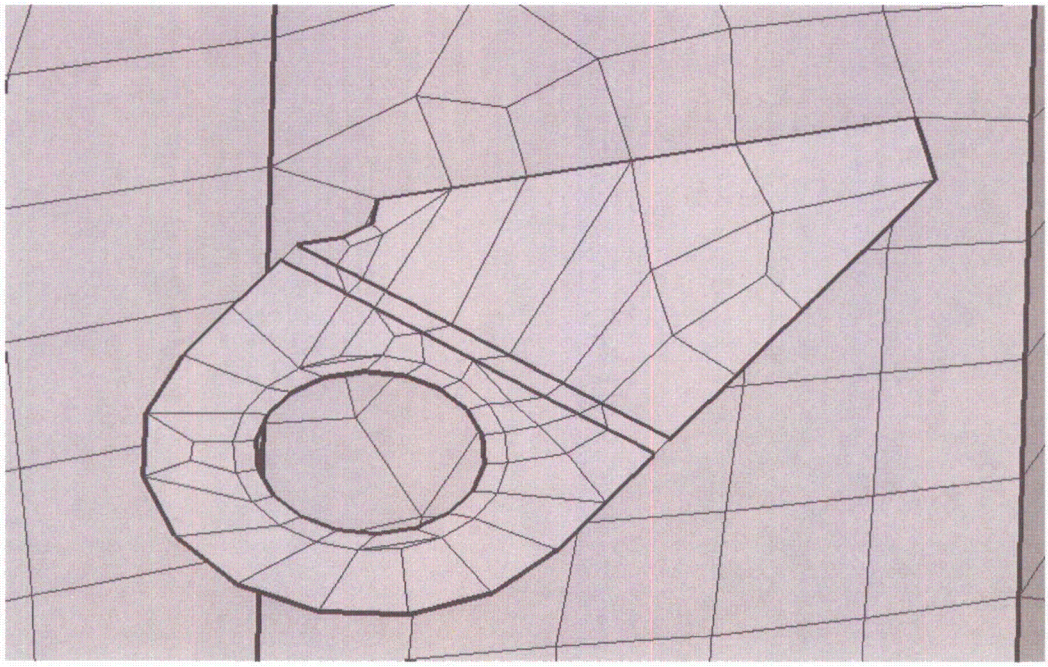

Figure 22. Unmodified Bracket

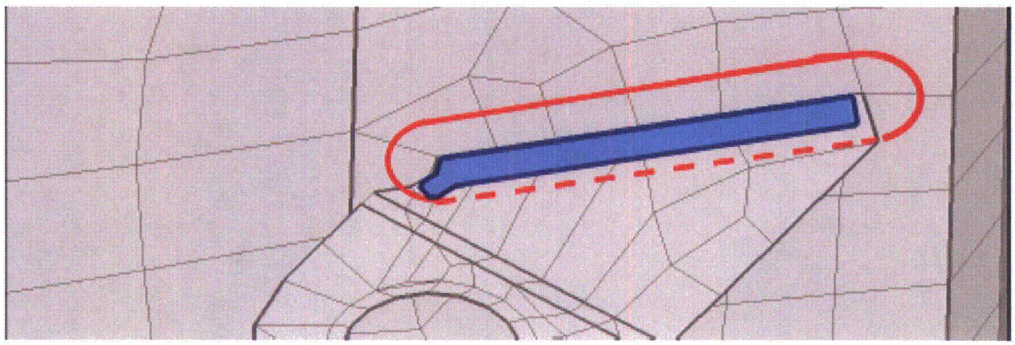

Reinforcement concept 1: Full reinforcement - weld plate to both side plate (red contour) and place reinforcement strip on bracket (blue region)

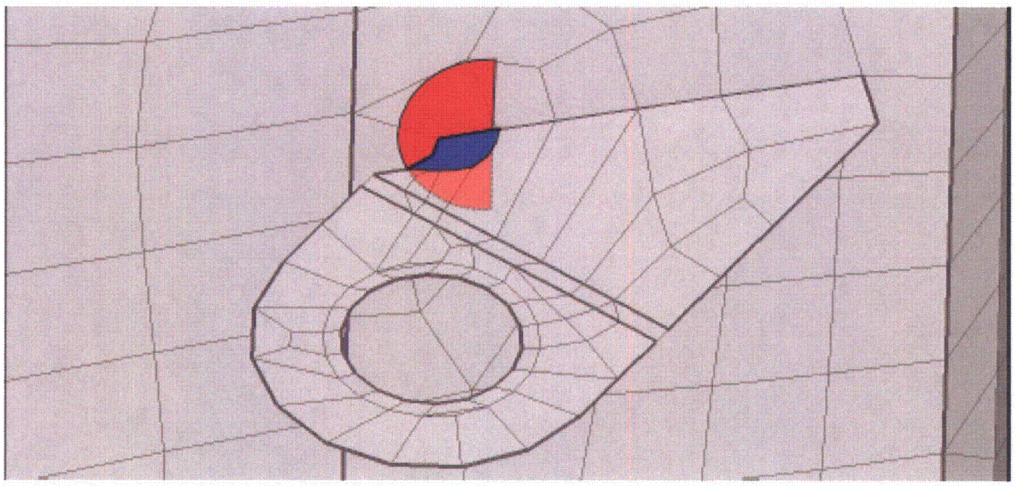

Reinforcement concept 2: Partial reinforcement – semi-circular plate one side plate (red) and reinforcement of re-entrant corner on support bracket (blue)

Figure 23. Potential reinforcement concepts for the lifting rod brackets.

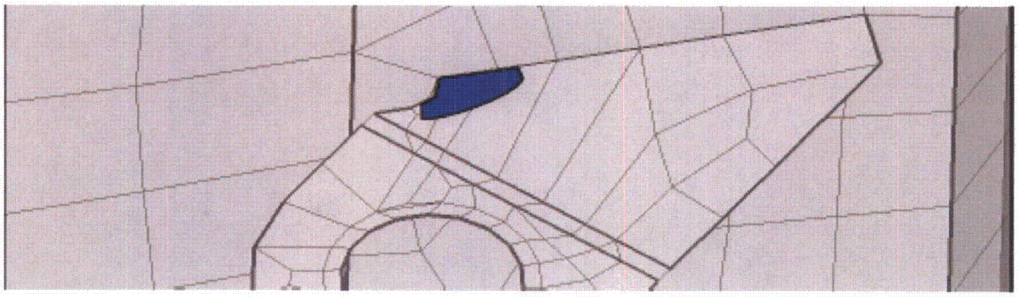

Reinforcement concept 3: Partial reinforcement – reinforcement plate welded on bracket to effectively increase local thickness.

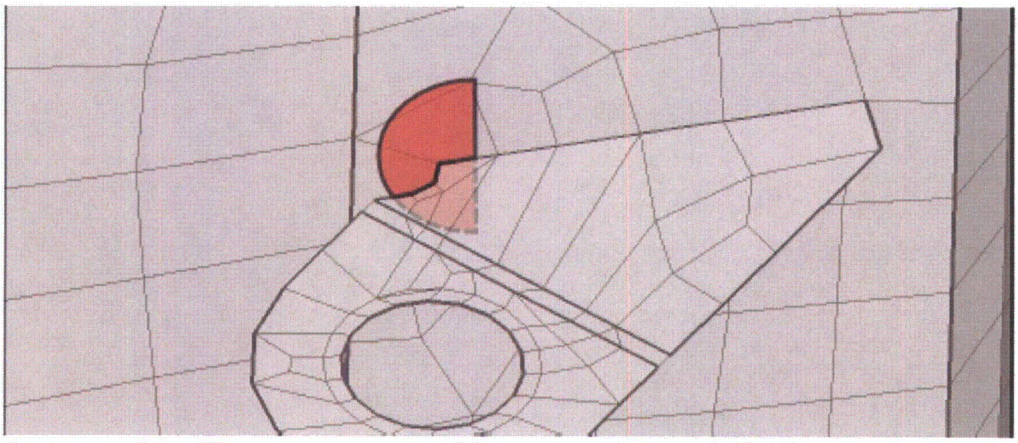

Reinforcement concept 4: Partial reinforcement – reinforcement plate welded on side plate in vicinity of high stress location.

Figure 23 (cont.). Potential reinforcement concepts for the lifting rod brackets.

Middle Hood/Reinforcement Strip (Group 2)

Application of the Rev. 4.1 acoustic loads produces stresses along the middle hood reinforcement strip that exceed target levels (SR-a=1.62). This strip was previously added to address indications on the outboard section of the middle hood. The high stresses occur on the 1/8" middle hood rather than within the much thicker strip (additional 3/8") and are caused by a pronounced response of the portion of the hood lying between the strip and the inboard closure plate (see Figure 24). The dominant signal frequency is 109.0 Hz which at the +10% shift excites a structural response at 119.9 Hz.

Local modifications to the weld line where the high stresses occur are unlikely to help in this case. For example, increasing the weld thickness merely shifts the high stress location slightly inboard to where the reinforcement begins. A more promising option is to place a second vertical strip on the middle hood positioned between the existing strip and the closure plate and coincident with the location where the mode causing the high stress has its peak amplitude. This modification suppresses the mode and associated stresses. Instead of placing a vertical strip, the entire section of the middle hood located between the existing reinforcement strip and the closure plate can be covered by a 3/8" curved plate welded about its perimeter to the hood. Since manufacture of the plate is straightforward and creating the attachment weld does not pose accessibility challenges, the cost and effort to implement this reinforcement option is comparable to that for the vertical strip.

A stress evaluation of this modification is performed by increasing the effective thickness of the hood by 3/8". Unit solution stresses of the complete steam dryer with this modified middle hood section (and also the other planned reinforcements – reinforced closure plate and added masses on the inner hoods as discussed below) are developed in the 30-250 Hz frequency range. This range is selected since: (i) it encompasses the frequency where stresses are highest and (ii) it ensures that any higher order modes occurring at higher frequencies are fully accounted for. Recalculation of the stresses at the Group 2 locations in Table 10 results in the considerably lowered stress in Table 12. Though more than adequate, this level of reinforcement seems excessive and a re-evaluation of the dryer using a ¼" or 1/8" rather than 3/8" curved plate over the middle hood section is recommended.

Table 12. Group 2 CLTP stresses after modification

Location	SRF	node	Pm	Pm+Pb	Sa	SR-P	SR-a	% Freq. Shift	Dom. Freq. [Hz]
2. Hood Reinforcement/Middle Hood	1	98275	195	342	200	40.78	34.32	-7.5	189.8
8. Hood Reinforcement/Middle Hood	1	90126	935	1244	208	9.94	33.07	5	51.2
9. Hood Reinforcement/Middle Hood	1	98268	328	520	240	26.82	28.56	-5	60.5
10. Hood Reinforcement/Middle Hood	1	90949	940	1030	303	9.89	22.63	2.5	146.4

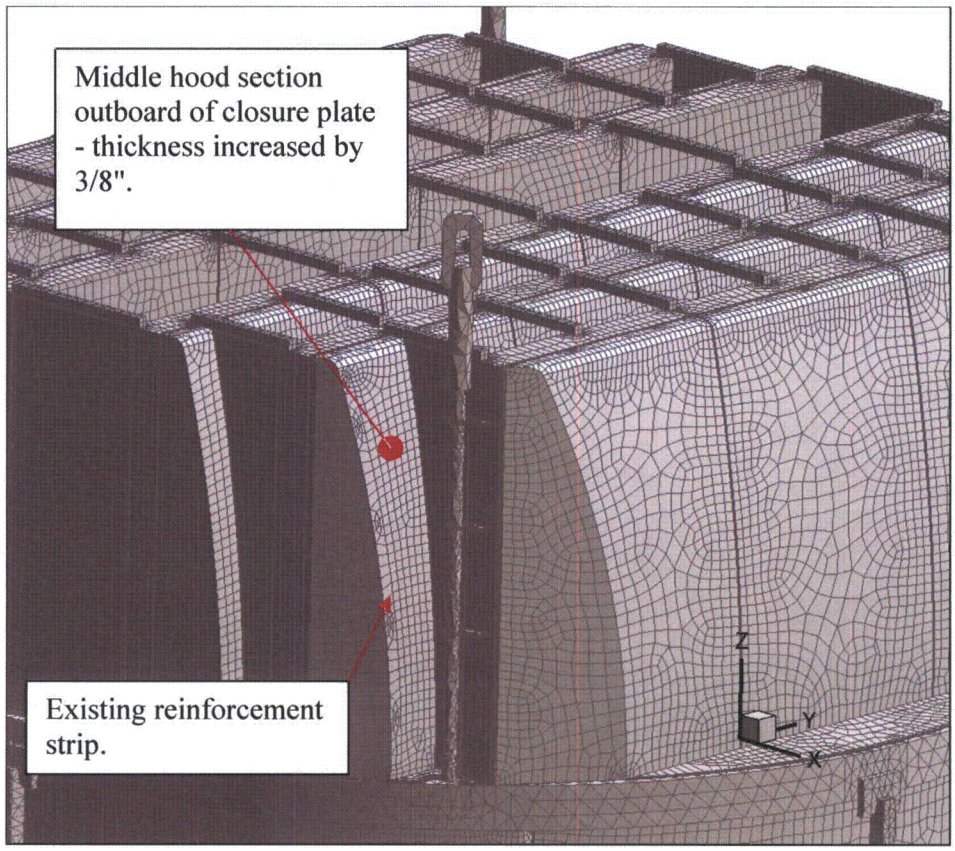

Figure 24. Middle hood section subject to modification and existing reinforcement strip.

Inner Hoods/Hood Support (Group 3)

The inner hoods and to a lesser extent also the middle hoods, show a strong stress response on the hood/hood support welds at 41 Hz and 51-54 Hz. The stresses result from strong vibrations of the central sections of the inner and middle hoods (see Figure 25). Since the acoustic loads on these hoods are relatively low, these vibrations are caused by transmission of loads from other steam dryer components such as the directly forced outer hoods. Previous sub-model analysis of the hood/hood support weld yielded a stress reduction factor of SRF=0.77 (this corresponds very closely to the ratio, 1.4/1.8=0.78, of the weld factor for a full penetration weld - the weld actually joining the hood and hood supports – of 1.4 and the default weld factor for a fillet weld of 1.8). Even with this SRF however, the stresses exceed EPU target levels. Since the welds, particularly at higher elevations, are difficult to access and reinforce it is necessary to pursue alternate modifications. One option is to stiffen the hood panels and suppress vibrations by adding reinforcement strips at the modal displacement response peaks. This would generally result in similar response modes occurring at upward-shifted natural frequencies. However, examination of the MSL signals in the vicinity of 52 Hz indicates that these signals increase with frequency so that an upward shift in the hood frequencies would place these frequencies into a range with stronger MSL signals.

Therefore the option proposed here is to add small (20lb) masses on the inner hoods. Specifically one such mass is added to each of four central inner hood sections as indicated in Figure 25. Each mass is located 18" below the top of the vane bank surface since this is approximately the reach length of a submerged diver welding the masses to the inner hoods. The masses themselves can be fashioned as 8" radius, ½" thick circular plates (equivalent area square plates or plates with alternate geometries can be employed with the preferred shape being dictated by welding considerations). The addition of the masses lowers the natural response frequencies and reduces the modal amplitudes (since the generalized masses of the participating modes are reduced). To evaluate the effectiveness of these added masses, unit solution stresses are generated in the 30-250 Hz frequency range with the added masses and also the reinforced closure plates and reinforced middle hood section described in the preceding section. When applying the same ACM Rev. 4.1 loads the stresses with these reinforcements all reduce to below target levels as indicated in Table 13.

Table 13. Group 3 CLTP stresses after modification

Location	SRF	node	Pm	Pm+Pb	Sa	SR-P	SR-a	% Freq. Shift	Dom. Freq. [Hz]
4. Hood Support/Inner Hood	1(b)	95636	1138	2683	2673	5.20	3.29	-2.5	45.5
5. Hood Support/Inner Hood	1(b)	95650	865	2373	2108	5.88	4.18	-10	51.3
6. Hood Support/Inner Hood	1(b)	95642	1136	2936	2889	4.75	3.05	-2.5	45.5

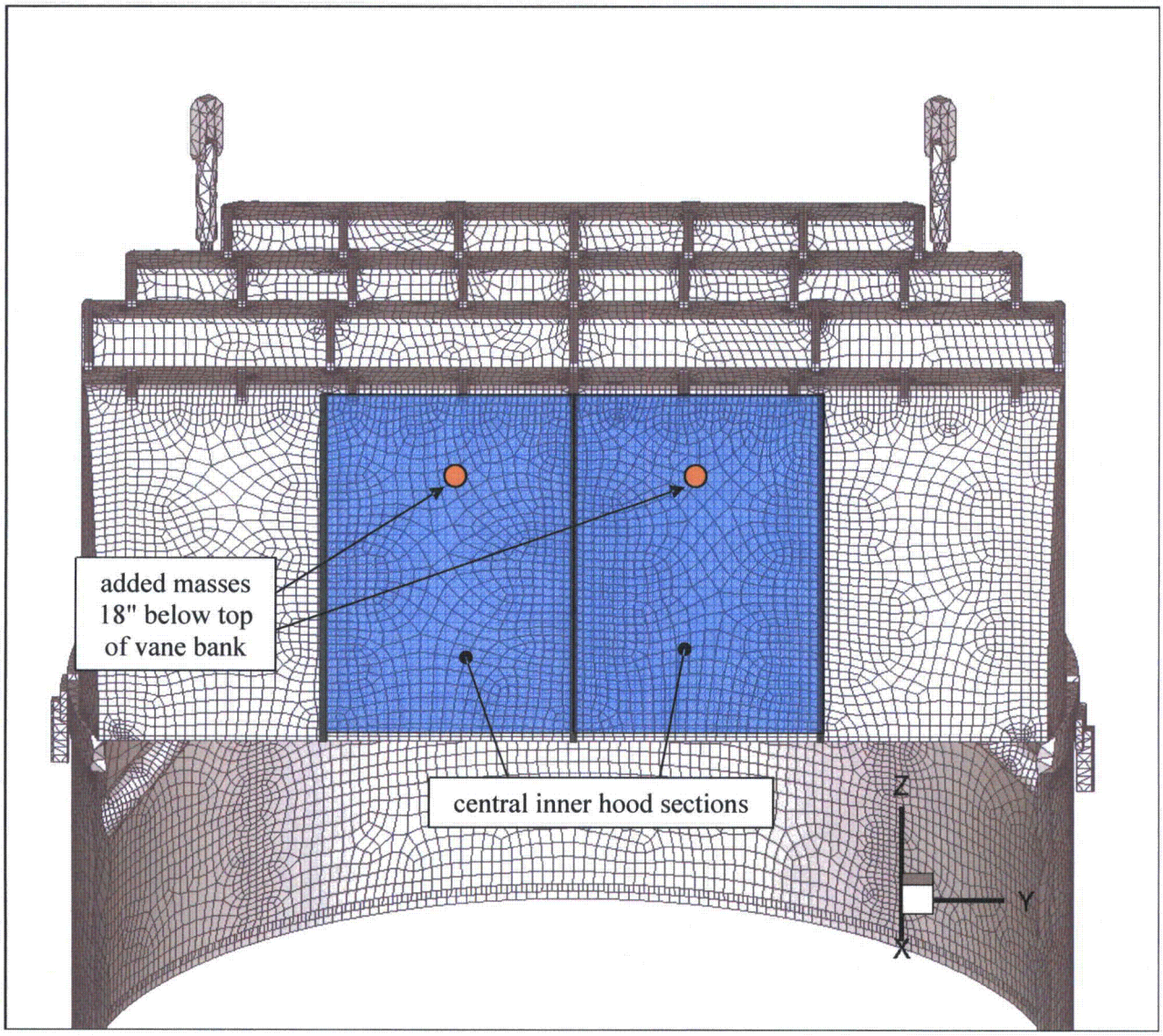

Figure 25. The inner hood sections (blue) whose response contributes to the high stresses on the central hood support/inner hood weld. Middle and outer hoods excluded from view to expose inner hood surfaces. Proposed masses are added 18" below the top of the vane bank.

Remaining Group 4

The stresses in the remaining group 4 do not change significantly with the modifications described above for groups 1-3. The unifying criterion for assembly of these diverse locations into a single group is that even without modification they all have stress ratios of 2.68 or higher. As such, there is a strong likelihood that the modifications outlined below will not be required. This follows upon recognizing that if measurement noise remains a significant primary contributor to the predicted stresses then, under the reasonable assumption that the noise levels will not change significantly with power increase, the stress ratios will increase at a somewhat lesser rate than inferred from a pure acoustics load. During power ascension, these locations can be processed using the actual measured signals at increased power levels and the exact same ACM Rev. 4.1 loads model and stress evaluation procedures utilized above. If the resulting stress ratios for these locations remain above 2.00 the power ascension process can continue; if the stress ratio reduces to below 2.00 then power ascension is halted and the modifications outlined below would be implemented in the subsequent outage. Consequently no additional modifications are considered mandatory to meet the required factor of 2 margin to the endurance limit for 120% EPU based on the application of the curve B of Fig I-9.2.2 in Appendix I in Section III of the ASME B&PV Code.

While not mandatory, scoping modification concepts for group 4 and preliminary access studies have nevertheless been carried out and have concluded that modifications to these locations feasible, achieve the 2.76 margin to the curve C endurance limit and can be implemented safely. However, these modifications are not considered warranted at this point based on: (i) application of ASME curve B noted above and (ii) preliminary data analysis indicating that the loads responsible for the reduced margin at these locations are governed primarily by noise. The latter assertion is supported by the [[(3)]] installed on MSL-D described in [6] and discussed in SIA calc 1000632.301[7]. With noise as a governing component the expectation is that the load will not increase with velocity squared and a significant margin above the EPU target of 2 will be demonstrated during power ascension testing.

In the event that this expectation is not realized the scoping modifications for group 4 are as follows. For locations 11 and 14 involving the common intersection between the hood, hood support and base plate a detailed evaluation of a weld reinforcement of this location has been conducted in [34] yielding a stress reduction factor of 0.63. With this reduction factor the stress ratio for this location increases to 3.27 which is well above the target value needed. This modification however, entails reinforcing the existing weld which, since the location must be accessed from underneath the dryer, exposes the diver to significant radiation dose. Therefore an alternative concept is also available consisting of a semi-circular stress relief hole cut from the bottom edge of the hood support near the high stress location. This concept is preferable to one involving welding since the cut-out can be generated using electrical discharge machining (EDM) that can be implemented remotely thus reducing diver dose to at most the period required to attach the device to the hood support. Only a 4% reduction in the local stress is required to meet the EPU target stress ratio. As shown in Appendix B, a stress reduction factor of 0.65 is obtained with the cut-out. The resulting alternating stress ratios at locations 11 and 14 with the stress relief cut-out are listed in the final column of Table 10 and shown to be well above 2.76.

The bottom of the submerged drain channel/skirt weld (locations 12 and 15 in Table 10) is easily accessible and can be reinforced by adding a wrap-around reinforcement weld to alleviate the stress. A similar reinforcement has been previously applied and a sub-model analysis carried out to estimate the stress reduction obtained with this reinforcement. The stress reduction factor calculated in [29] was SRF=0.58 and the entries in the final column of Table 10 for these locations are obtained using this

value. While the sub-modeling technology is somewhat different than the one used in Appendix A, the stress reduction factor needed here to meet margin is only 0.96 or lower which is easily achievable with the additional weld reinforcement.

To address location 13 involving the weld joining the middle hood and hood support, it is proposed to place masses similar to, but smaller than, the masses added to the inner hoods to suppress similar high stresses on the inner hood/hood support weld. When the 20 lb masses are added to the inner hoods the limiting stress ratio on the inner hood/hood support welds increased from 2.17 to 3.05 (a 28.8% stress reduction). The middle hoods have identical thickness and similar dimensions to the inner hoods and also respond in similar modes. Hence addition of a mass at the same 18" depth measured from the top of the vane bank is expected to achieve a comparable stress reduction. Note that a much lesser reduction of 2.9% is needed to raise the stress ratio from 2.68 to 2.76. Given that the percent stress reduction is about ten times smaller than that for the inner hoods, it follows that: (i) the stress reduction using masses placed on the middle hoods is easily achievable and (ii) the reduction is obtainable using considerably smaller (5-10 lb) masses. Based on this reasoning, the last entry in the last column in Table 10, while not definitive, is reasonably estimated to exceed 2.76.

Table 14. Summary of non-mandatory modifications proposed for locations in group 4.

Location	Modification	node	SR-a	
			Pre-modification	Post-Modification
11. Hood Support/Outer Base Plate/Middle Backing Bar	Cut-out in hood support (SRF=0.65)	95428	2.65	4.08
14. Hood Support/Outer Cover Plate/Outer Hood	Cut-out in hood support (SRF=0.65)	95267	2.71	4.17
12. Submerged Drain Channel/Submerged Skirt	Wrap around weld (SRF=0.58)	93430	2.65	4.57
15. Submerged Drain Channel/Submerged Skirt	Wrap around weld (SRF=0.58)	84597	2.72	4.69
13. Hood Support/Middle Hood	Added mass	96022	2.68	>2.76

7. Conclusions

A frequency-based steam dryer stress analysis has been used to calculate high stress locations and stress ratios for the Nine Mile Point Unit 2 steam dryer at CLTP load conditions using plant measurement data. A detailed description of the frequency-based methodology and the finite element model for the NMP Unit 2 steam dryer is presented. The CLTP loads obtained in a separate acoustic circuit model [11] including end-to-end bias and uncertainty for both the ACM [11] and FEA were applied to a finite element model of the steam dryer consisting mainly of the ANSYS Shell 63 elements and brick continuum elements.

The measured CLTP loads are applied without subtracting low power data and using the ACM Rev. 4.1 model to predict acoustic loads. The resulting stress histories were analyzed to obtain maximum and alternating stresses at all nodes for comparison against allowable levels. These results are tabulated in Table 9 of this report. With reinforcements of the closure plates, closure plate attachment welds and lifting rod brace/side plate welds the minimum alternating stress ratio taken over all frequency shifts is SR-a=1.56 which is insufficient to meet the target EPU stress margin. Therefore additional modifications, described in Section 6, are added. With these modifications the limiting alternating stress ratio increases to greater than SR-a=2.76 for all locations warranting modification. The stress ratio associated with maximum stress intensities varies weakly with frequency shift and assumes a minimum value of SR-P=1.25.

Review of the stress margin identifies a group of locations (group 4 in Section 6) that that has a minimum alternating stress ratio SR-a=2.65 which corresponds to the steam flow for 117.5% EPU conditions. No additional modifications are considered mandatory to meet the required factor of two margin to the endurance limit for 120% EPU based on the application of the curve B of Fig I-9.2.2 in Appendix I of Section III in the ASME B&PV Code for the group 4 locations. In addition, supplemental measurements using the [[(3)]] installed on MSL-D described in [6] and discussed in SIA calc 1000632.301 [7] indicate that noise in the frequency intervals when scaled using the velocity squared rule is biasing the stress ratios high. Based on noise as the governing component of the load, the load is not expected to increase with a velocity squared scaling so that the final margin is expected to remain well above the factor of 2 at 120% EPU. While modification concepts for the group 4 locations are developed and presented, complete stress evaluations for the modifications are not considered warranted given that a factor of two margin is demonstrated using the ASME code endurance limits applicable to this location. It is also anticipated, based on the [[(3)]] supplemental data on MSL-D, that power ascension testing will demonstrate substantial margin without modification of the group 4 locations.

8. References

1. *ASME Boiler and Pressure Vessel Code, Section III, Subsection NG (2007).*
2. Continuum Dynamics, Inc. (2005) *Methodology to Determine Unsteady Pressure Loading on Components in Reactor Steam Domes (Rev. 6).* C.D.I. Report No. 04-09 (Proprietary).
3. Continuum Dynamics, Inc. (2010) *ACM Rev. 4.1: Methodology to Predict Full Scale Steam Dryer Loads from In-Plant Measurements.* C.D.I. Report No. 10-09P (Proprietary), June.
4. Continuum Dynamics, Inc. (2010) *Acoustic and Low-Frequency Hydrodynamic Loads at CLTP Power Level on Nine Mile Point Unit 2 Steam Dryer to 250 Hz Using ACM Rev. 4.1.* C.D.I. Report No. 10-10P (Proprietary), June.
5. Continuum Dynamics, Inc. (2009) *Stress Assessment of Nine Mile Point Unit 2 Steam Dryer at CLTP and EPU Conditions, Rev. 1.* C.D.I. Report No. 09-26P (Proprietary), December.
6. Continuum Dynamics, Inc. (2010) *Development and Qualification of Instrumentation to Determine Unsteady Pressures in Piping, Revision 0.* 10-06P, March.
7. Structural Integrity Associates, Inc. (2010) *Nine Mile Point Unit 2 Main Steam Line Strain Gage Data Reduction (Rev. 0).* SIA Calculation Package No. 1000632.301, May.
8. Continuum Dynamics, Inc. (2007) *Methodology to Predict Full Scale Steam Dryer Loads from In-Plant Measurements, with the Inclusion of a Low Frequency Hydrodynamic Contribution.* C.D.I. Report No. 07-09P (Proprietary).
9. Structural Integrity Associates, Inc. (2009) *Nine Mile Point Unit 2 Steam Dryer Closure Plates Analysis Results.* SIA Letter Report No. 0900895.401 Revision 0, August 21.
10. Structural Integrity Associates, Inc. (2008) *Nine Mile Point Unit 2 Main Steam Line Strain Gage Data Reduction.* SIA Calculation Package No. NMP-26Q-302.
11. Continuum Dynamics, Inc. (2008) *Acoustic and Low Frequency Hydrodynamic Loads at CLTP Power Level on Nine Mile Point Unit 2 Steam Dryer to 250 Hz, Rev. 2.* C.D.I. Report No. 08-08P (Proprietary).
12. ANSYS, *Release 10.0 Complete User's Manual Set, (http://www.ansys.com).*
13. Continuum Dynamics, Inc. (2007) *Response to NRC Request for Additional Information on the Hope Creek Generating Station, Extended Power Uprate.* RAI No. 14.110.
14. Continuum Dynamics, Inc. (2008) *Stress Assessment of Hope Creek Unit 1 Steam Dryer Based on Revision 4 Loads Model, Rev. 4.* C.D.I. Report No. 07-17P (Proprietary).
15. Press, W.H., et al., *Numerical Recipes.* 2 ed. 1992: Cambridge University Press.
16. Structural Integrity Associates, Inc. (2008) *Flaw Evaluation and Vibration Assessment of the Nine Mile Point Unit 2 Steam Dryer for Extended Power Uprate Operating Conditions.* Report No. 0801273.401.
17. Continuum Dynamics, Inc. (2008) *Stress Assessment of Browns Ferry Nuclear Unit 1 Steam Dryer, Rev. 0.* C.D.I. Report No. 08-06P (Proprietary).
18. O'Donnell, W.J., *Effective Elastic Constants For the Bending of Thin Perforated Plates With Triangular and Square Penetration Patterns.* ASME Journal of Engineering for Industry, 1973. **95**: p. 121-128.
19. de Santo, D.F., *Added Mass and Hydrodynamic Damping of Perforated Plates Vibrating In Water.* Journal of Pressure Vessel Technology, 1981. **103**: p. 175-182.
20. Idel'chik, I E. and E. Fried, *Flow Resistance, a Design Guide for Engineers.* 1989, Washington D.C.: Taylor & Francis. pg. 260.
21. Continuum Dynamics, Inc. (2007) *Dynamics of BWR Steam Dryer Components.* C.D.I. Report No. 07-11P.
22. U.S. Nuclear Regulatory Commission (2007) *Comprehensive Vibration Assessment Program for Reactor Internals During Preoperational and Initial Startup Testing.* Regulatory Guide 1.20, March.

23. Weld Research Council (1998) *Fatigue Strength Reduction and Stress Concentration Factors For Welds In Pressure Vessels and Piping*. WRC Bulletin 432.
24. Pilkey, W.D., *Peterson's Stress Concentration Factors, 2nd ed.* 1997, New York: John Wiley. pg. 139.
25. Lawrence, F.V., N.-J. Ho, and P.K. Mazumdar, *Predicting the Fatigue Resistance of Welds.* Ann. Rev. Mater. Sci., 1981. **11**: p. 401-425.
26. General Electric (GE) Nuclear Energy, *Supplement 1 to Service Information Letter (SIL) 644, "BWR/3 Steam Dryer Failure," September 5.* 2003.
27. Tecplot, Inc. (2004) *Documentation: Tecplot User's Manual Version 10 Tecplot, Inc.*, October.
28. GE Nuclear Energy (2006) *Browns Ferry Nuclear Plant Units 1, 2, and 3 Steam Dryer Stress, Dynamic, and Fatigue Analysis for EPU Conditions.* GE-NE-0000-0053-7413-R4-NP.
29. Structural Integrity Associates, Inc. (2008) *Shell and Solid Sub-Model Finite Element Stress Comparison, Rev. 2.* Calculation Package, 0006982.301, Oct. 17.
30. Continuum Dynamics, Inc. (2008) *Stress Assessment of Browns Ferry Nuclear Unit 2 Steam Dryer with Outer Hood and Tie-Bar Reinforcements, Rev. 0.* C.D.I. Report No. 08-20P (Proprietary).
31. Structural Integrity Associates, Inc. (2008) *Comparison Study of Substructure and Submodel Analysis using ANSYS.* Calculation Package, 0006982.304, December.
32. Continuum Dynamics, Inc. (2009) *Response to NRC Round 23 RAI EMCB 201/162 part c.* January.
33. Continuum Dynamics, Inc. (2009) *Compendium of Nine Mile Point Unit 2 Steam Dryer Sub-Models Away From Closure Plates* C.D.I. Technical Note No. 09-16P (Proprietary), August.
34. Continuum Dynamics, Inc. (2010) *Sub-model analysis of the Nine Mile Point steam dryer high stress location at node 85723, hood - base plate - hood support – backing bar junction.* C.D.I. Letter Report, April.

Appendix A Sub-modeling and Modification of Closure Plates

[[

[3]]]

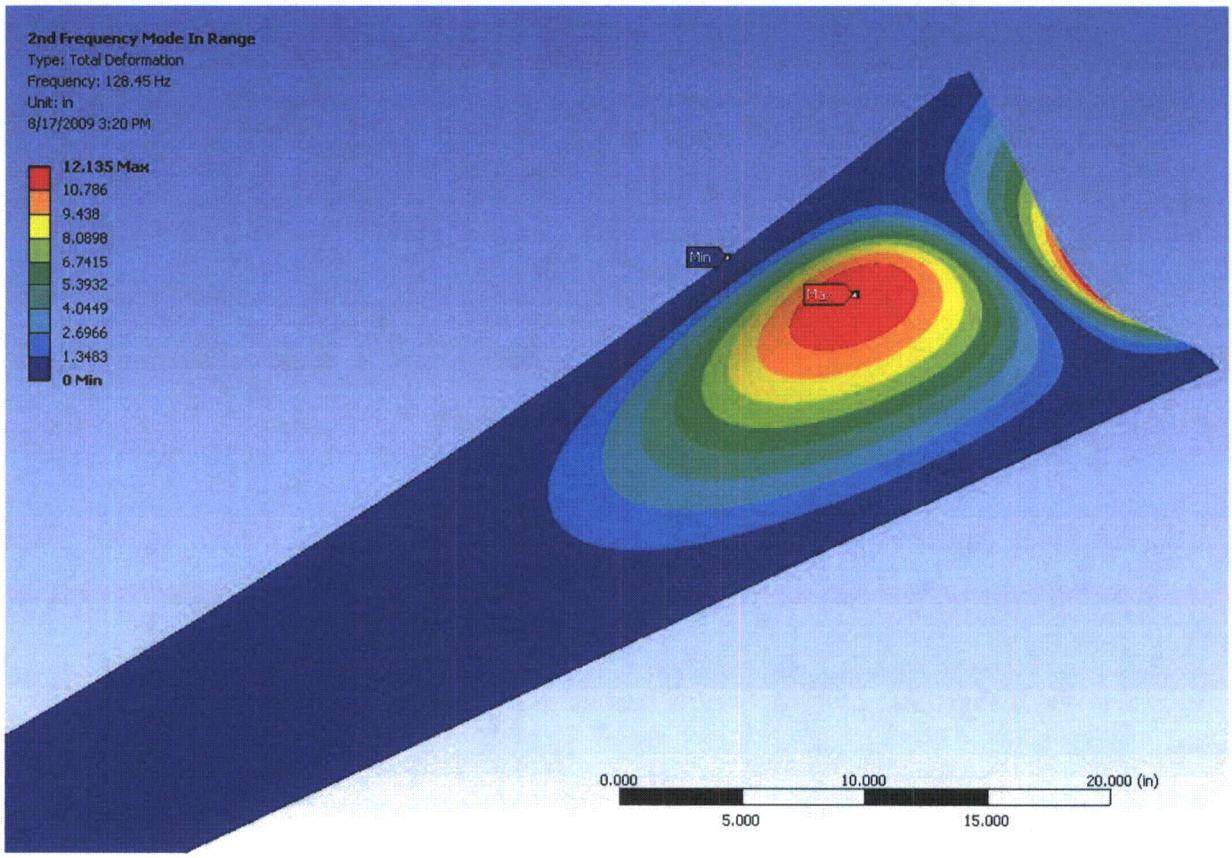

Figure 26: Second mode shape (f=128.45 Hz) of unmodified closure plates

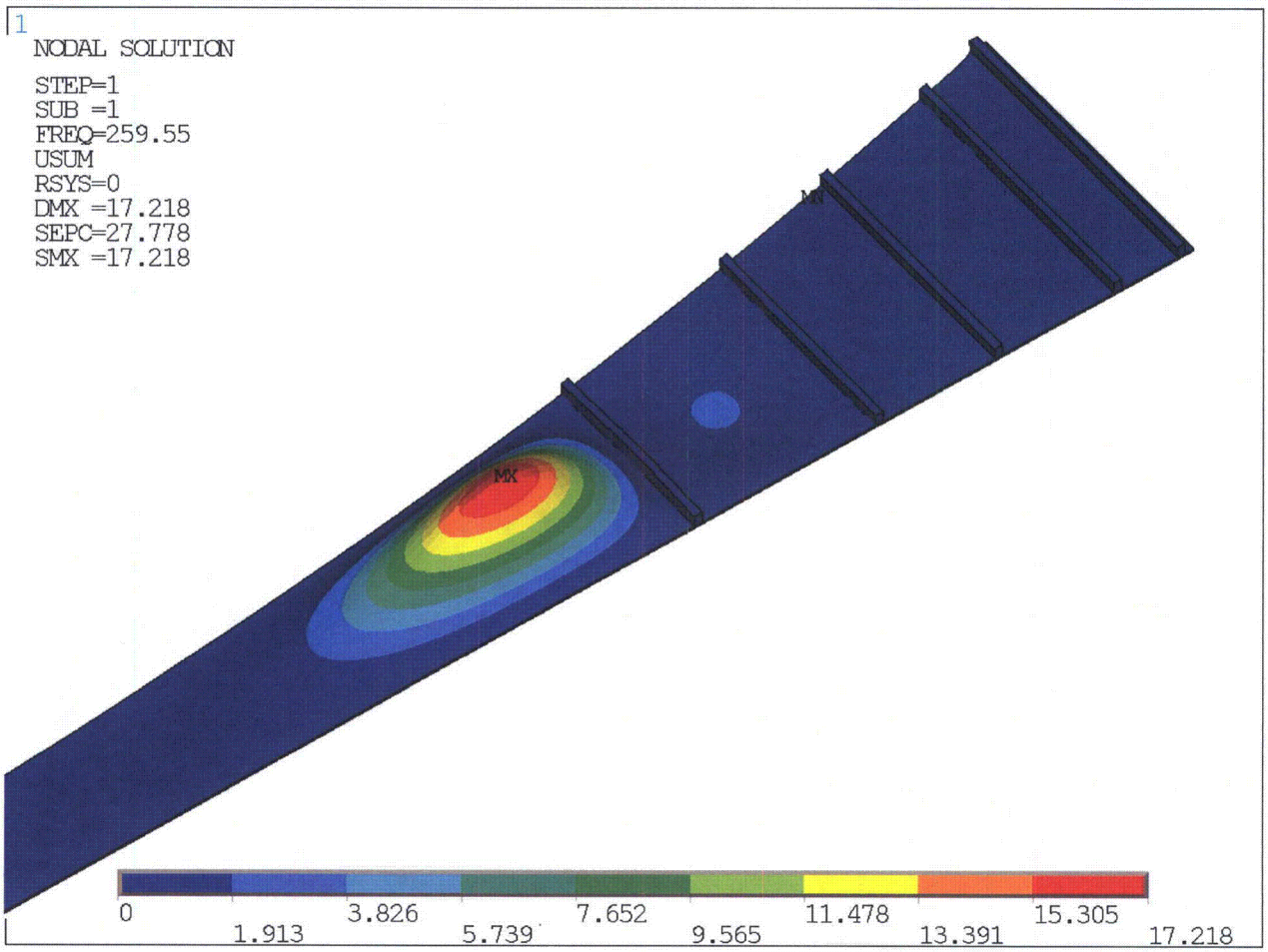

Figure 27: Fundamental mode shape (f=259.6 Hz) of modified closure plate.

[[

[3]]]

[[

[3]]]

The sub-modeled locations together with the calculated stress reduction factors are given in Table 15. For each location depictions of the shell and solid element-based sub-models are given together with the applied loads/moments and resulting stresses. This is followed by a summary of the linearization paths and the limiting linearized stresses. The calculation of the stress reduction factor concludes the presentation for each location.

Table 15. List of sub-model locations

Location	x	y	z	node	Stress reduction factor
Top Thick Plate/Side Plate/Closure Plate/Top Plate	47.1	-108.6	88	101175	0.62
Closure Plate/Middle Hood	-63.8	85.2	72.5	91605	0.71
Closure Plate/Inner Hood	28.8	-108.6	87	95172	0.86
Side Plate/Closure Plate/Exit Top Perf/Exit Mid Top Perf	-47.1	108.6	74.5	100327	0.88

Note: The side plate/closure plate connection involving nodes 101175 and 100327 is reinforced on the interior side with a 0.25" weld. The hood/closure plate weld involving nodes 91605 and 95172 is reinforced on the interior side with a 0.125" weld.

Sub model Node 101175

The sub-model for this node located at the top of the vertical weld joining the closure plate to the vane bank is shown in Figure 28a and involves five different components. The extracted forces are shown in Figure 28b. The shell sub-model stress distribution is shown in Figure 28c with a maximum (i.e., the maximum taken over all components and surfaces – top, bottom and middle) stress intensity stress at the location of 3362 psi. The corresponding solid sub-model together with mesh details and the stress distribution resulting when the same loads used in the shell sub-model are applied, are shown in Figure 29. Finally, the stress intensity linearization paths and corresponding linearized stresses extracted from the solid model are shown in Figure 30 and tabulated in Table 16. The limiting linearized stress in the solid sub-model is **2088 psi**. Comparing this value against the one obtained in the shell sub-model (**3362 psi**) yields the stress reduction factor: 2088/3362 = **0.62**.

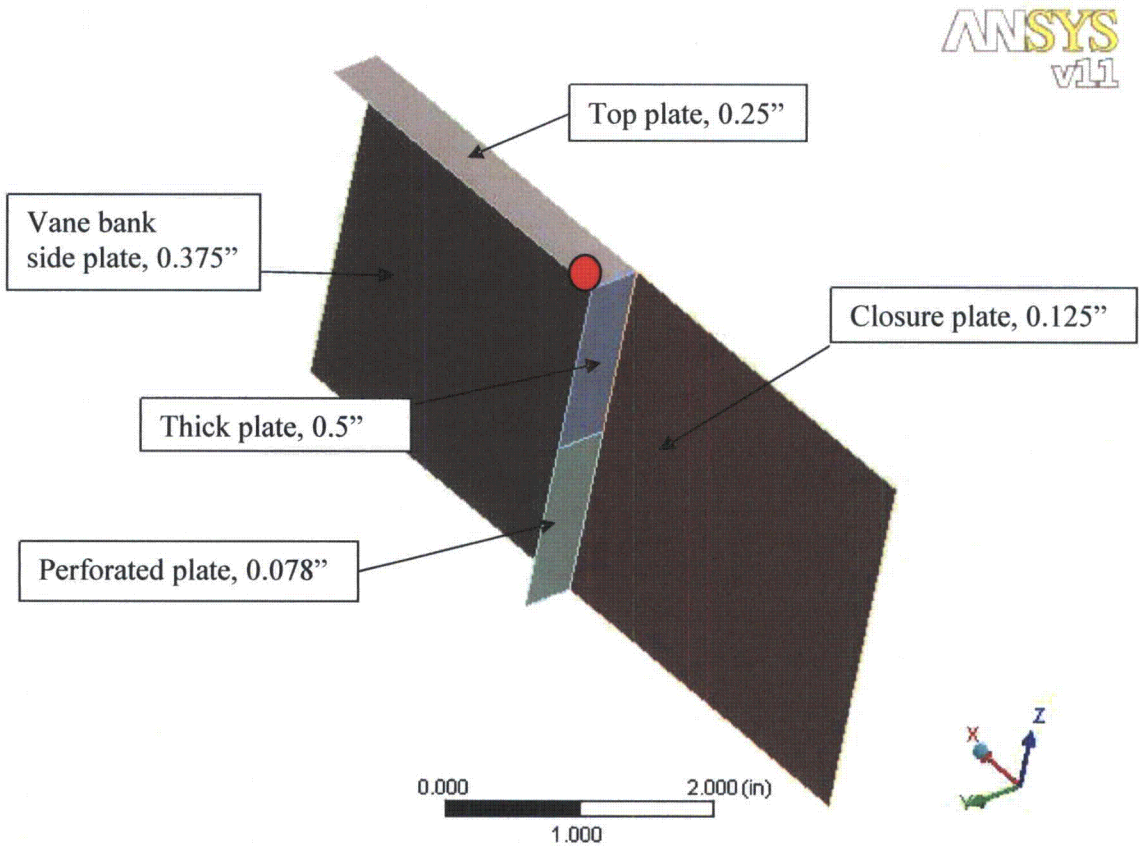

Figure 28a. Shell sub-model node 101175.

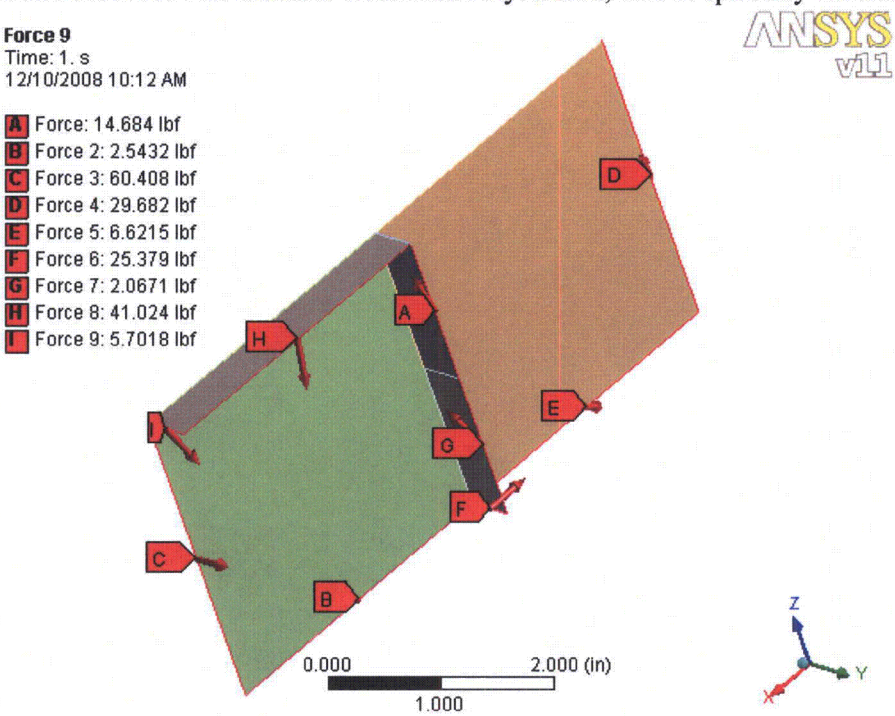

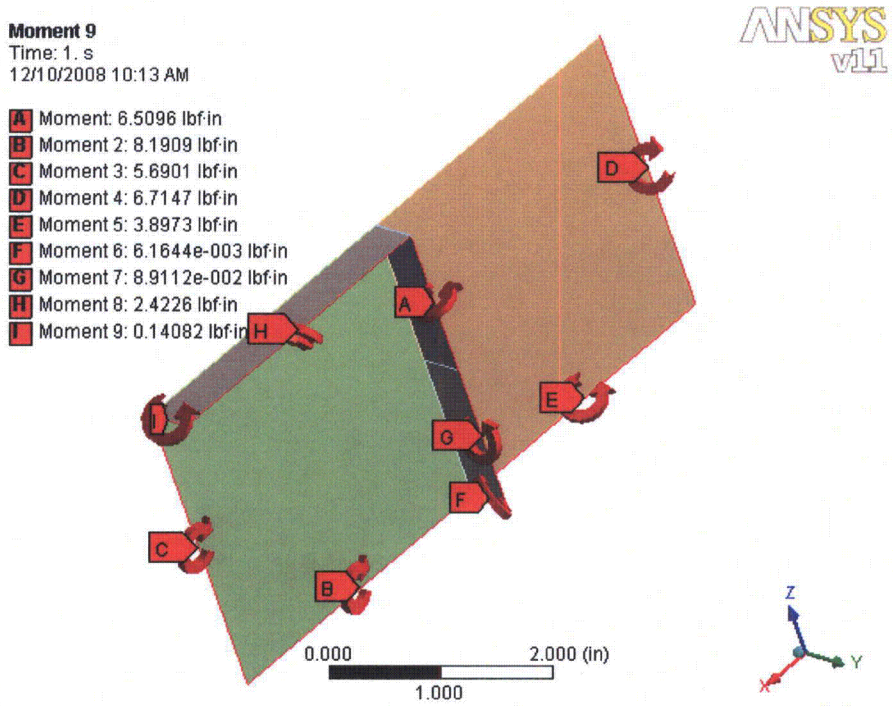

Figure 28b. Forces and moments.

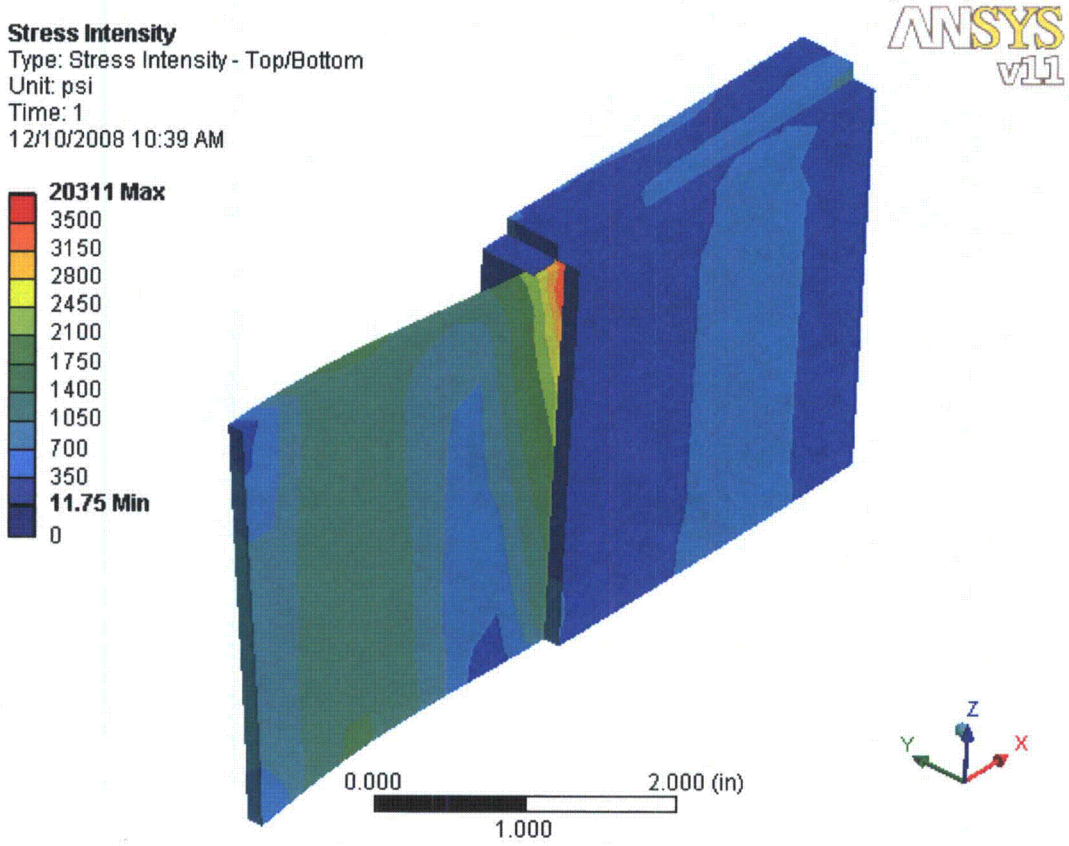

Figure 28c. Shell sub-model stress contours. Stress intensity: 3362 psi.

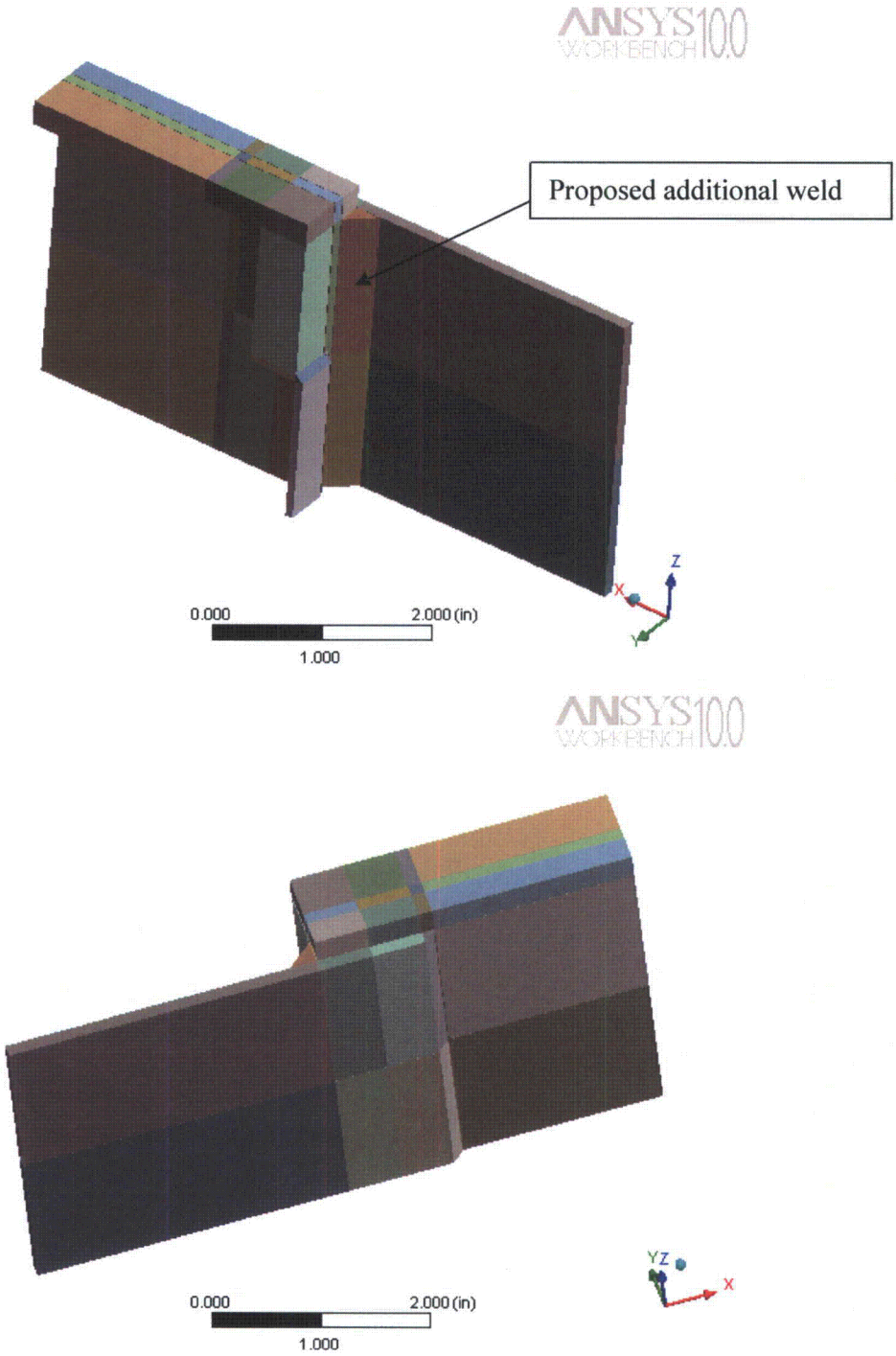

Figure 29a. Solid model geometry.

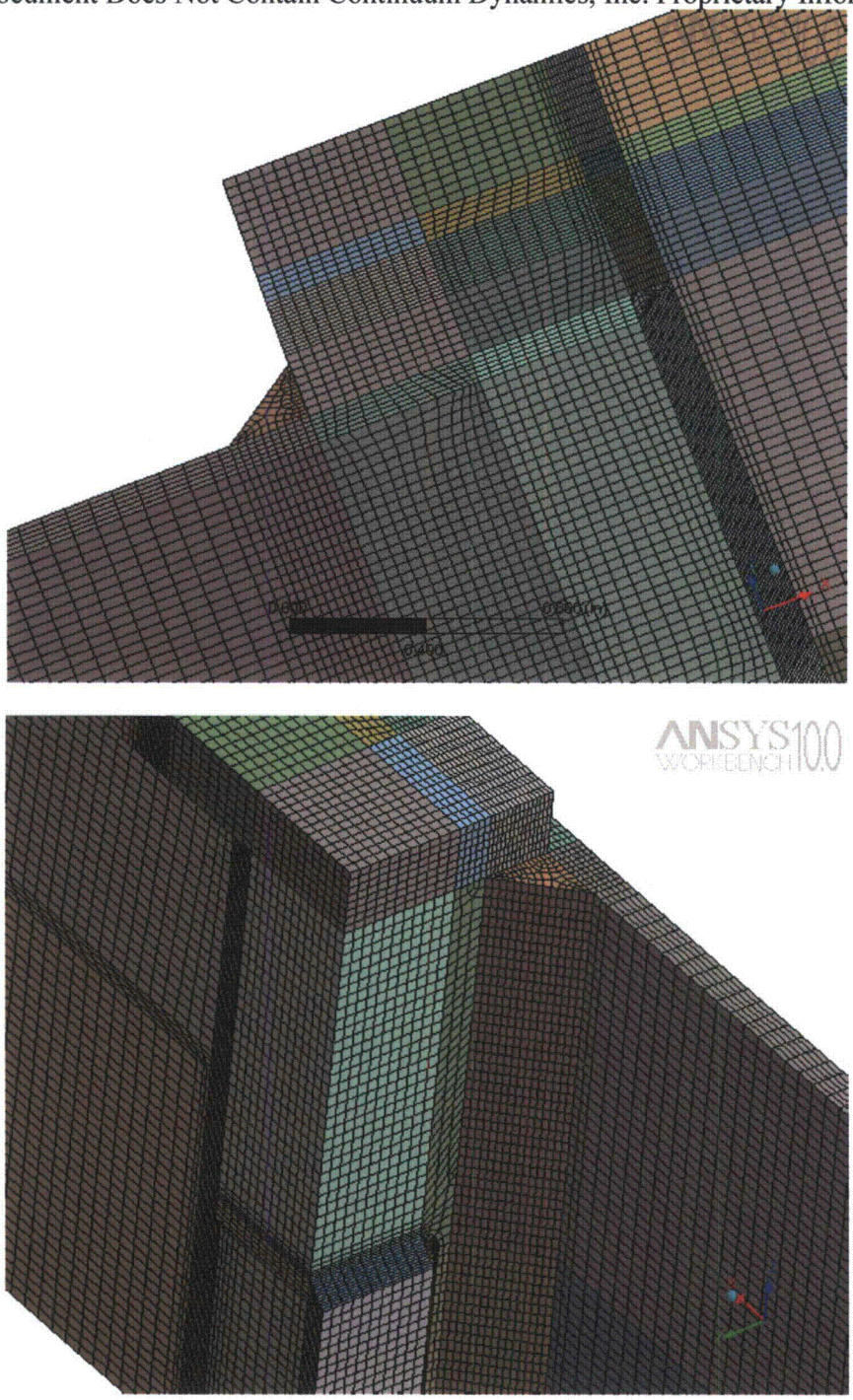

Figure 29b. Mesh overview. Mesh parameters: 748,327 nodes, 176,028 elements.

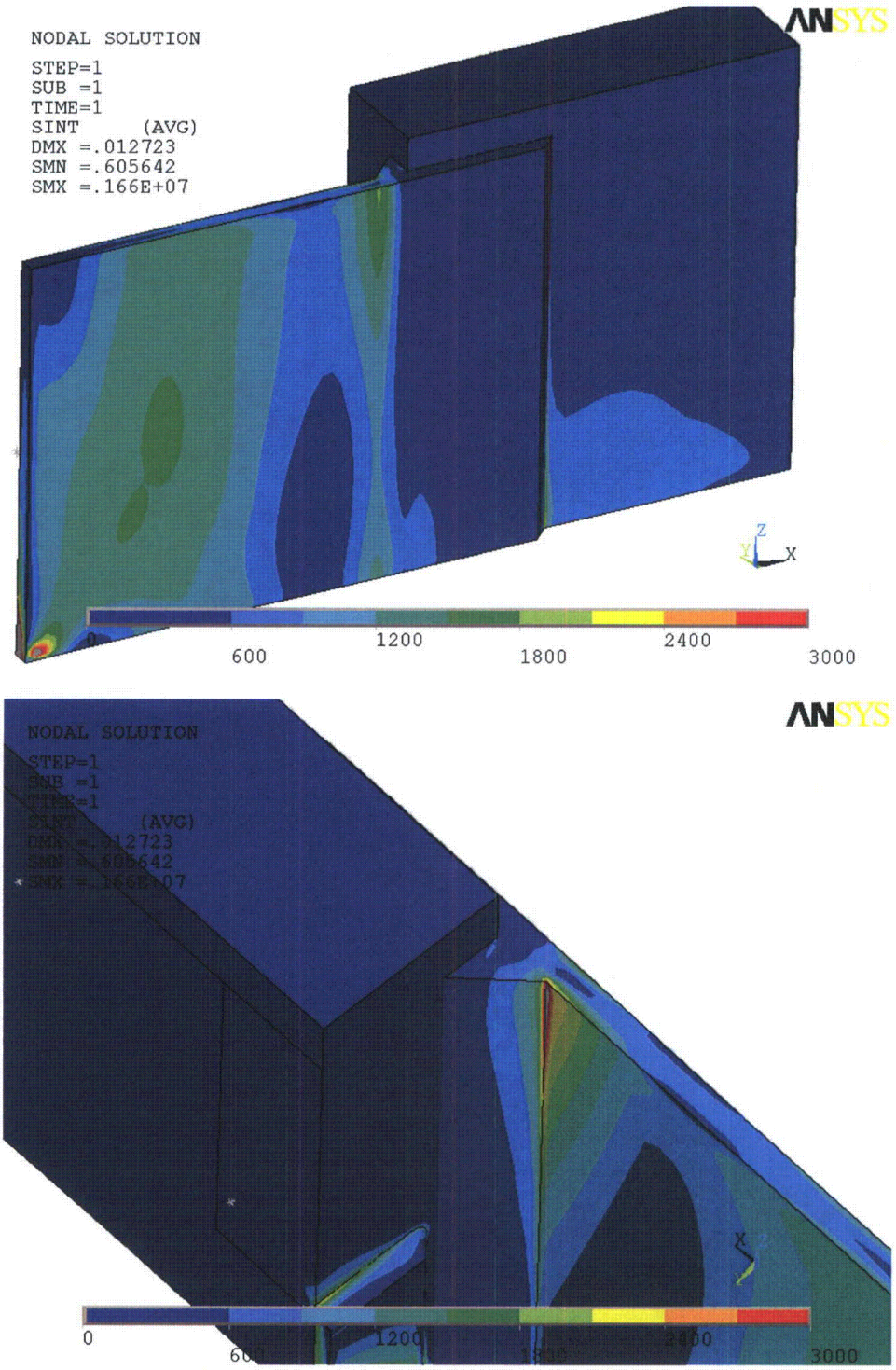

Figure 29c. Stress intensity contours (total) in solid sub-model.

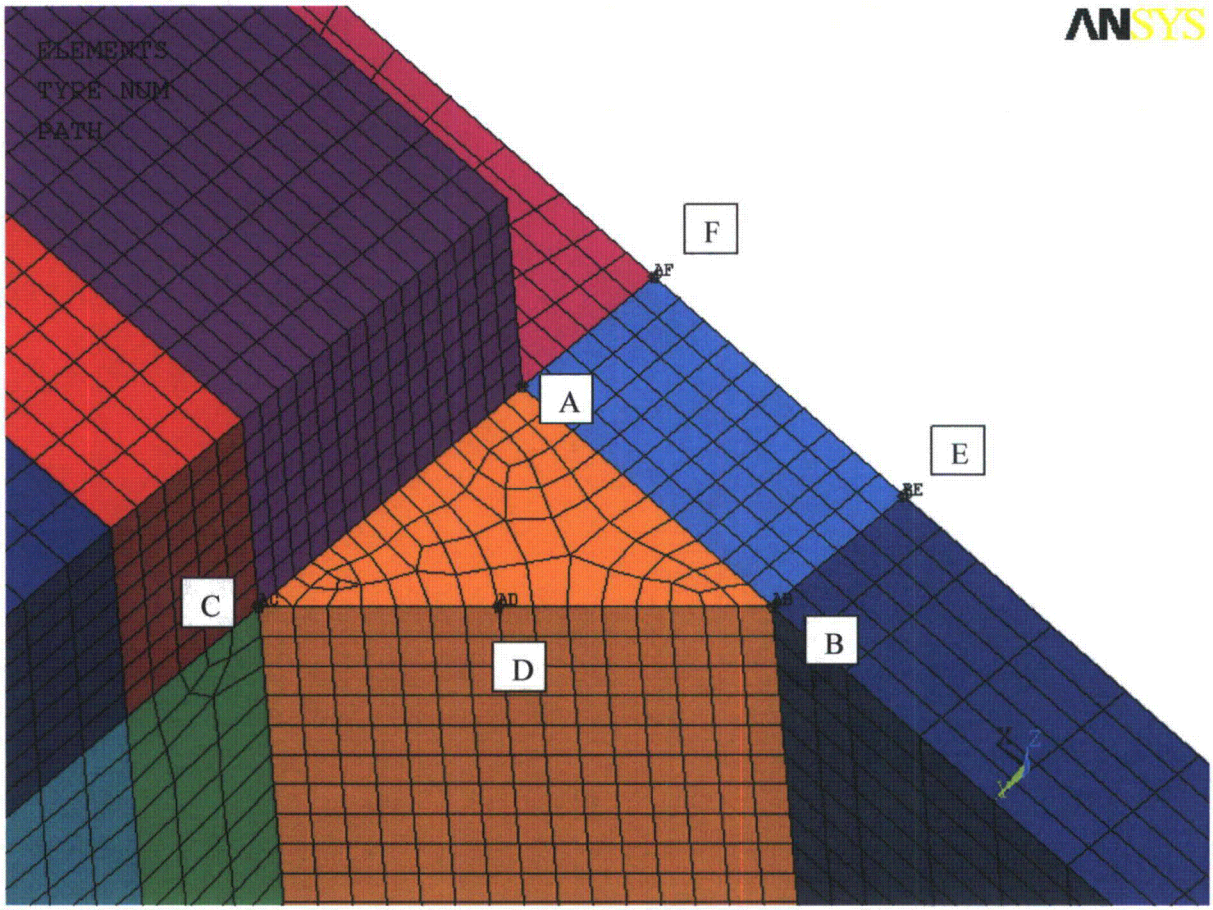

Figure 30. Linearization paths for sub-model node 101175.

Table 16. Linearized stresses along the linearization paths shown in Figure 30.

Path	Membrane + bending linearized stress intensity, psi
AB	1605
AC	710
AD	689
AF	492
BE	2088

Sub model node 91605.

The sub-model for this node located on the weld connecting the closure plate to the hood is shown in Figure 31a and involves two different components - the hood and closure plate. The extracted forces are shown in Figure 31b. The shell sub-model stress distribution is shown in Figure 31c with a maximum (i.e., the maximum taken over all components and surfaces – top, bottom and middle) stress intensity stress at the location of 3176 psi. The stresses in the corners are neither singularities nor due to constraint forces (they arise regardless of where the model is supported). When the sub-model mesh is refined these stresses do not grow. Instead they essentially retain their coarse level values but extend over a smaller range (i.e., over one element). A mathematical explanation for this behavior indicates that the localized stress is due to the local imbalance (due to discretization error) in the applied shear loads. Thus to equilibrate the applied in-plane stresses on the edges a jump in element stress is required. The same behavior generally occurs when non-equal shear stresses are applied near the corner.

The solid sub-model, mesh and stresses are shown in Figure 32 and, the stress intensity linearization paths and corresponding linearized stresses extracted from the solid model are shown in Figure 33 and tabulated in Table 17. The limiting linearized stress in the solid sub-model is **2254 psi**, which, when compared against the one obtained in the shell sub-model (**3176 psi**) yields the stress reduction factor: 2254/3176 = **0.71**.

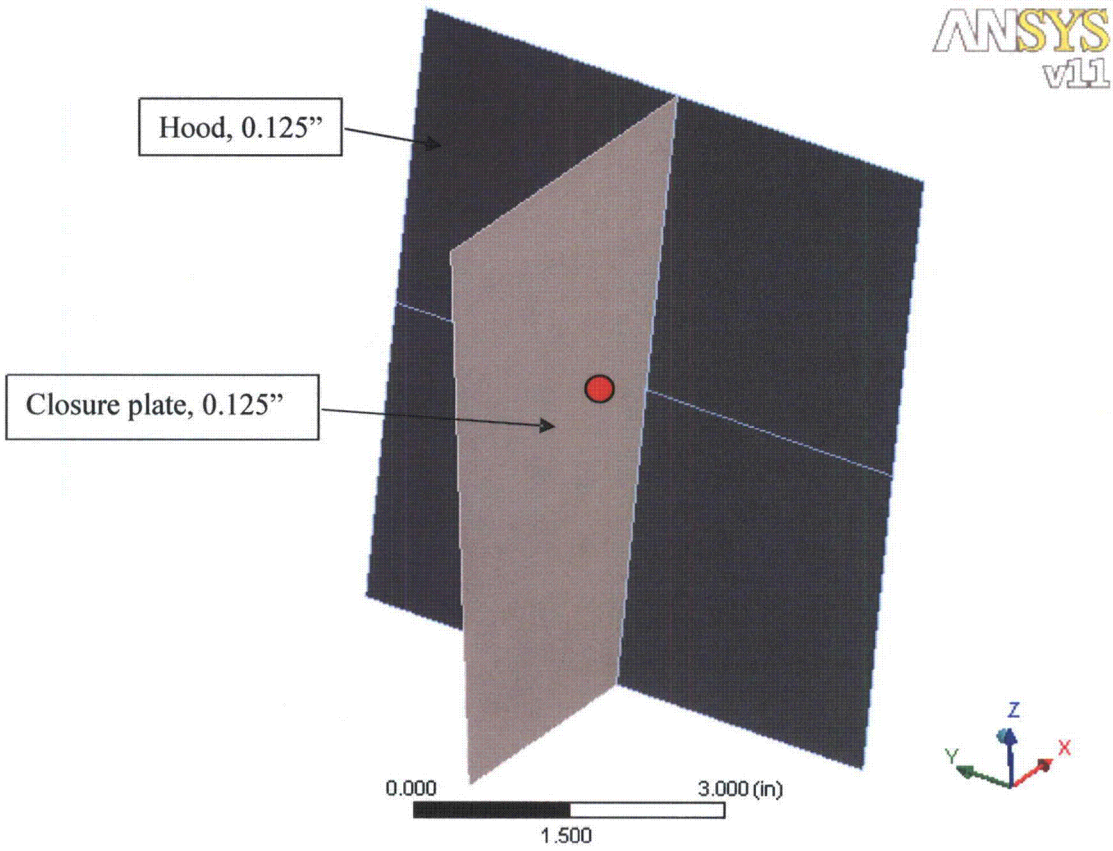

Figure 31a. Shell sub-model node 91605.

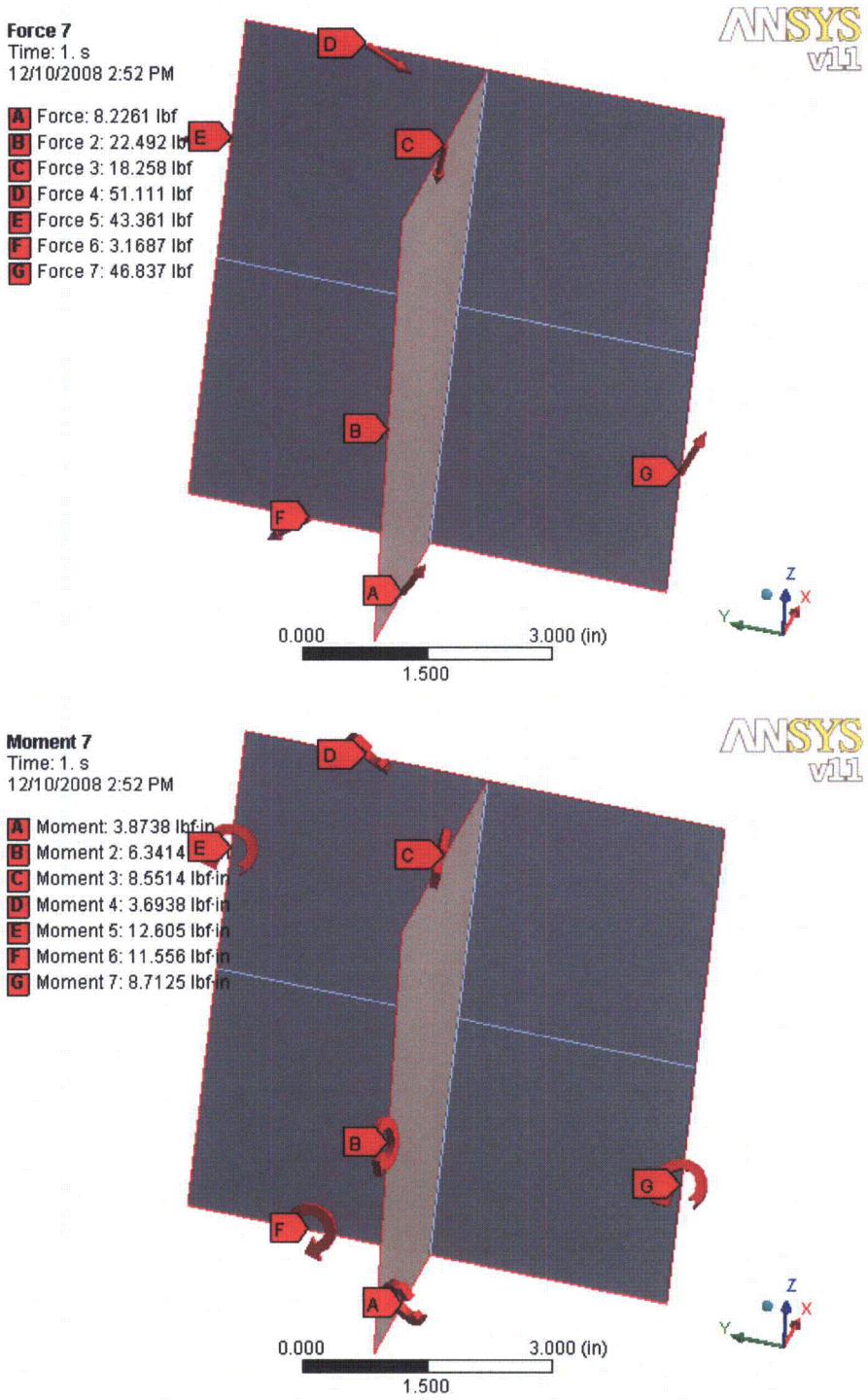

Figure 31b. Forces and moments.

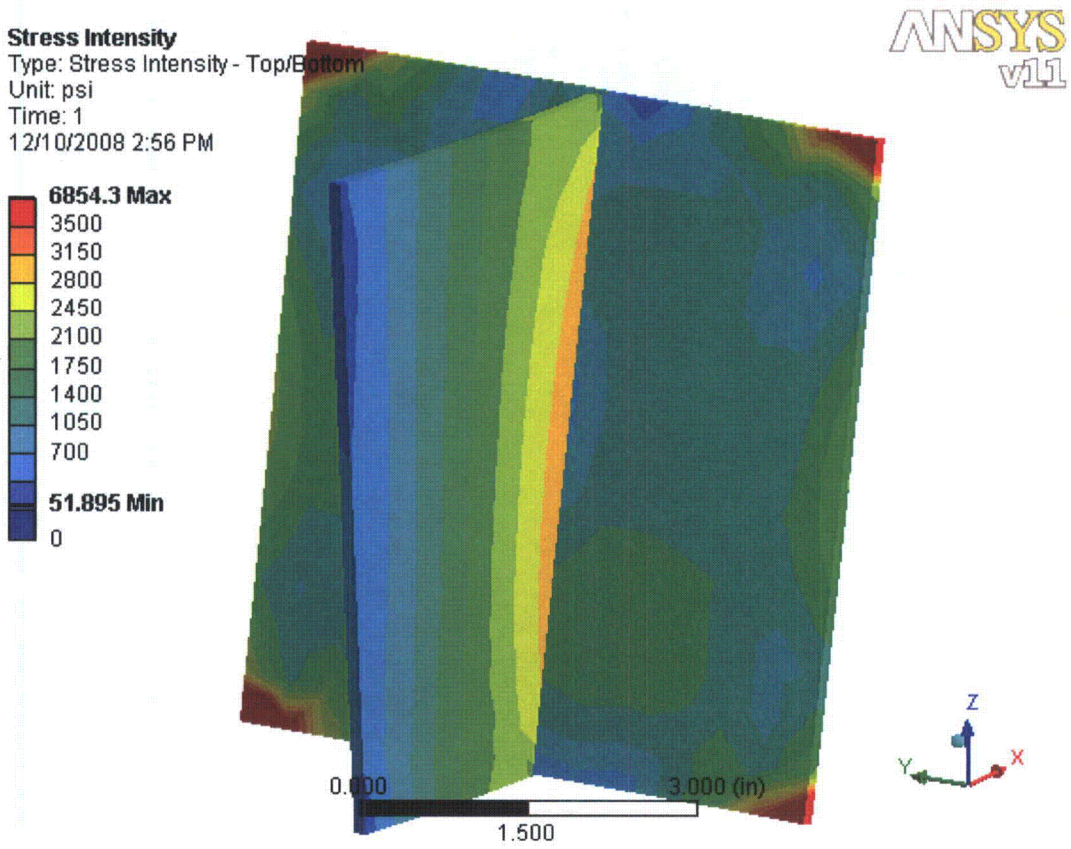

Figure 31c. Shell sub-model stress contours. Stress intensity: 3176 psi.

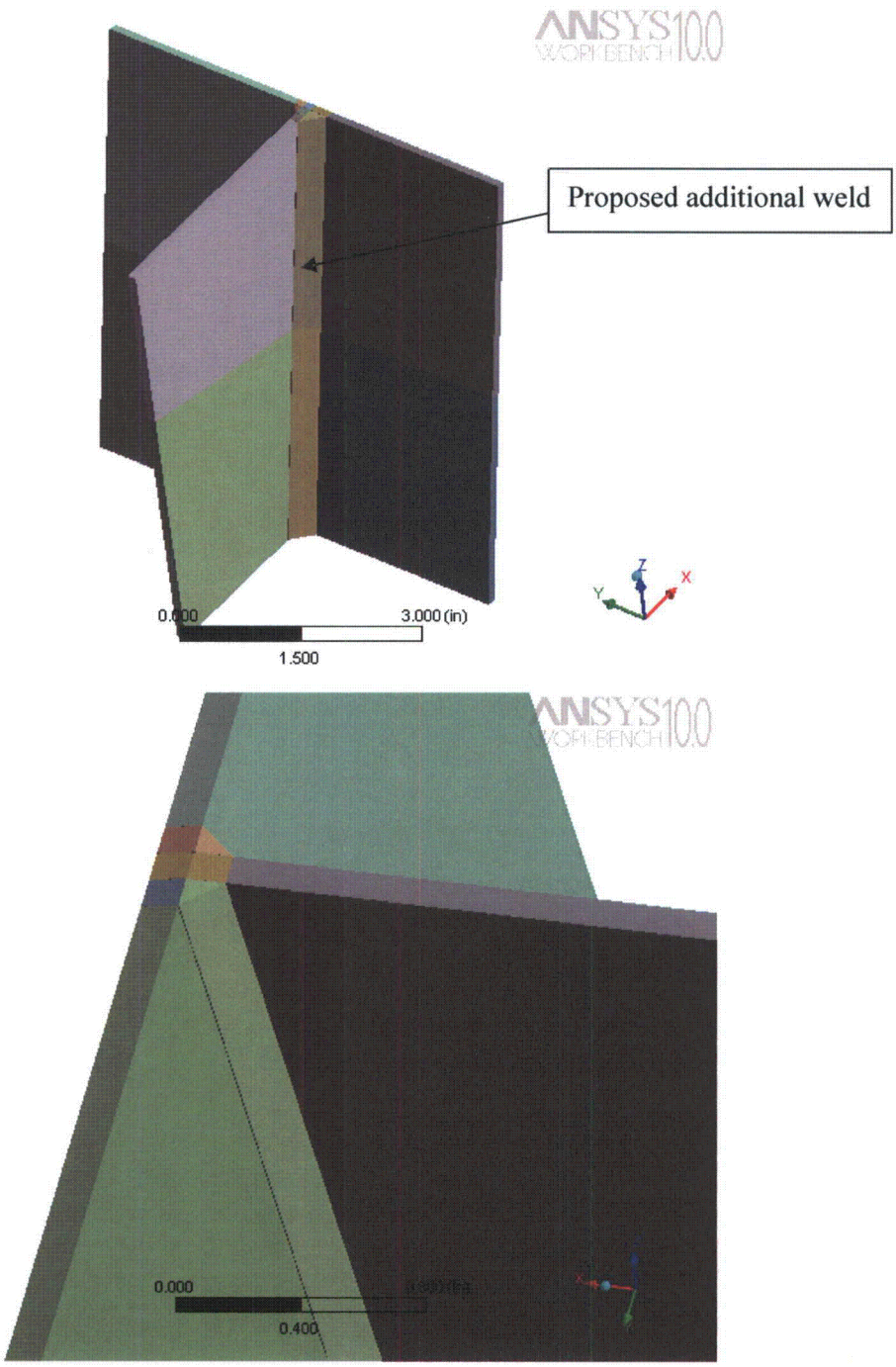

Figure 32a. Solid model geometry.

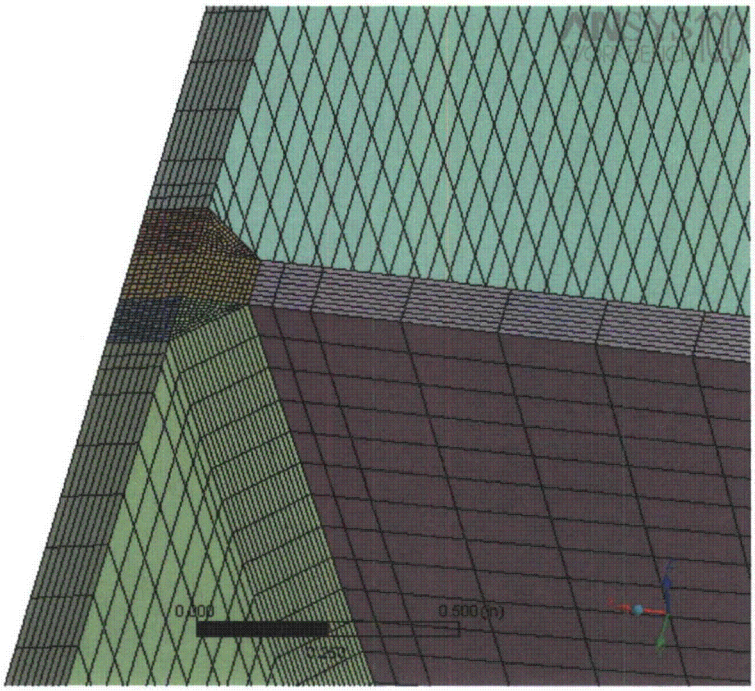

Figure 32b. Mesh overview.

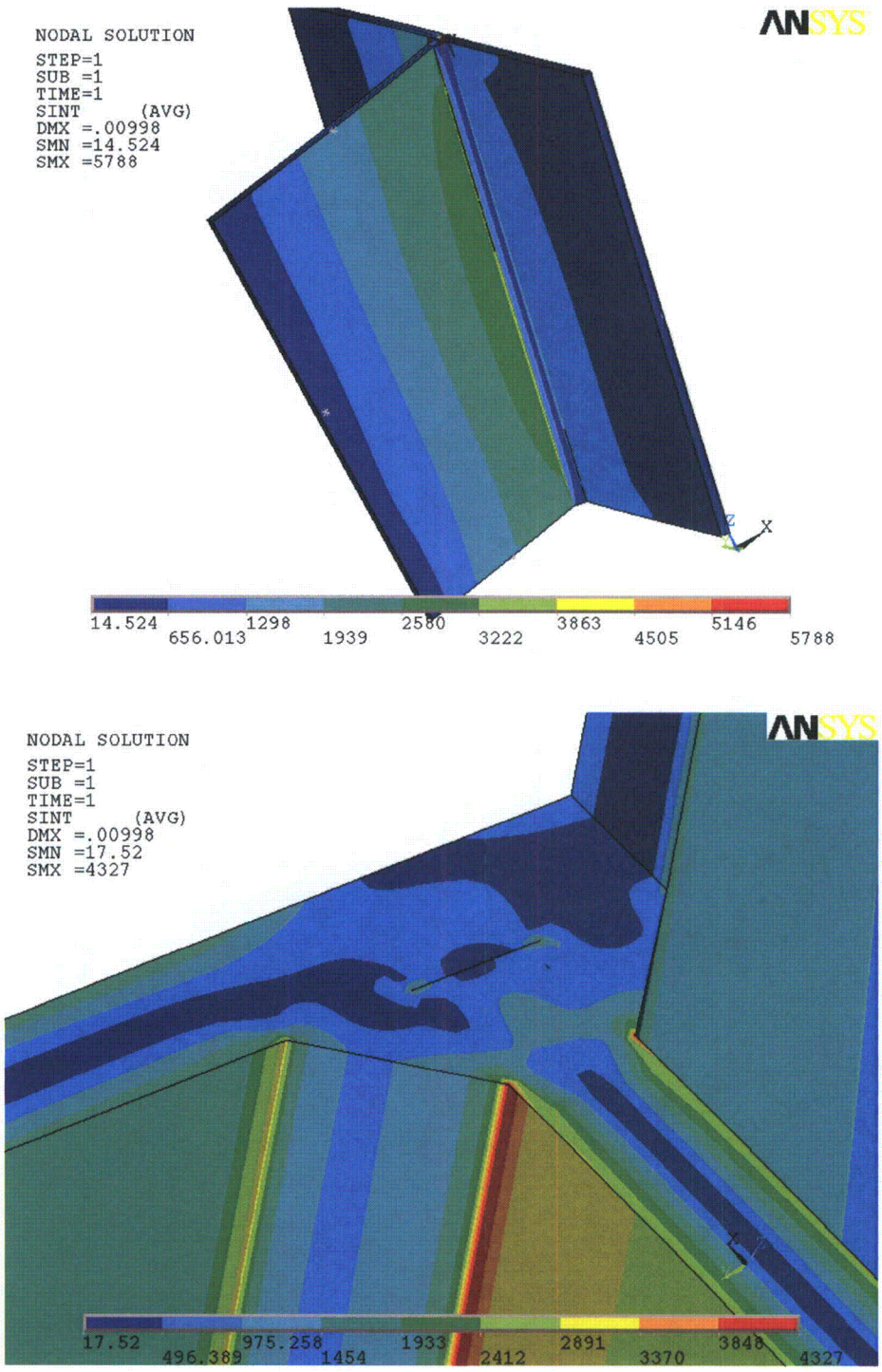

Figure 32c. Stress intensity contours (total) in solid sub-model. Part of structure is removed in the lower figure to show internal stress distribution.

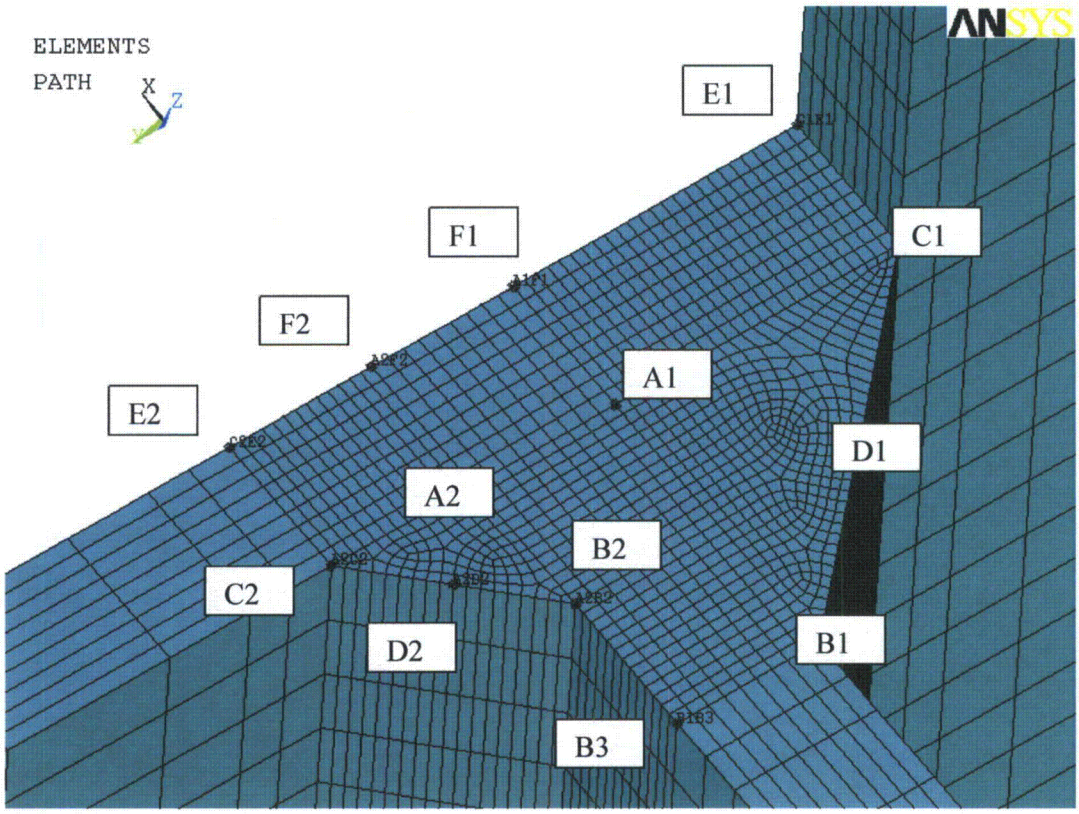

Figure 33. Linearization paths for sub-model node 91605.

Table 17. Linearized stresses along the linearization paths shown in Figure 33.

Path	Membrane + bending linearized stress intensity, psi
A1-B1	2254
A1-C1	1891
A1-D1	1261
A1-F1	822
C1-E1	1899
A2-B2	2170
A2-C2	1154
A2-D2	1160
A2-F2	867
C2-E2	930
B1-B2	2139

Sub model node 95172.

The sub-model for this node located at the top of the weld connecting the closure plate to the curved hood is shown in Figure 34a and again involves only two distinct components - the curved hood and closure plate. The extracted forces are shown in Figure 34b and the shell sub-model stress distribution is shown in Figure 34c with a maximum (i.e., the maximum taken over all components and surfaces – top, bottom and middle) stress intensity stress at the location of 3198 psi. The solid sub-model, mesh and stresses are shown in Figure 35 and, the stress intensity linearization paths on the original and added weld are shown in Figure 36. The corresponding linearized stresses extracted from the solid model are tabulated in Table 18. The limiting linearized stress in the solid sub-model is **2762 psi**. The corresponding value in the shell sub-model is **3198 psi** so that the stress reduction factor is 2762/3198 = **0.86**.

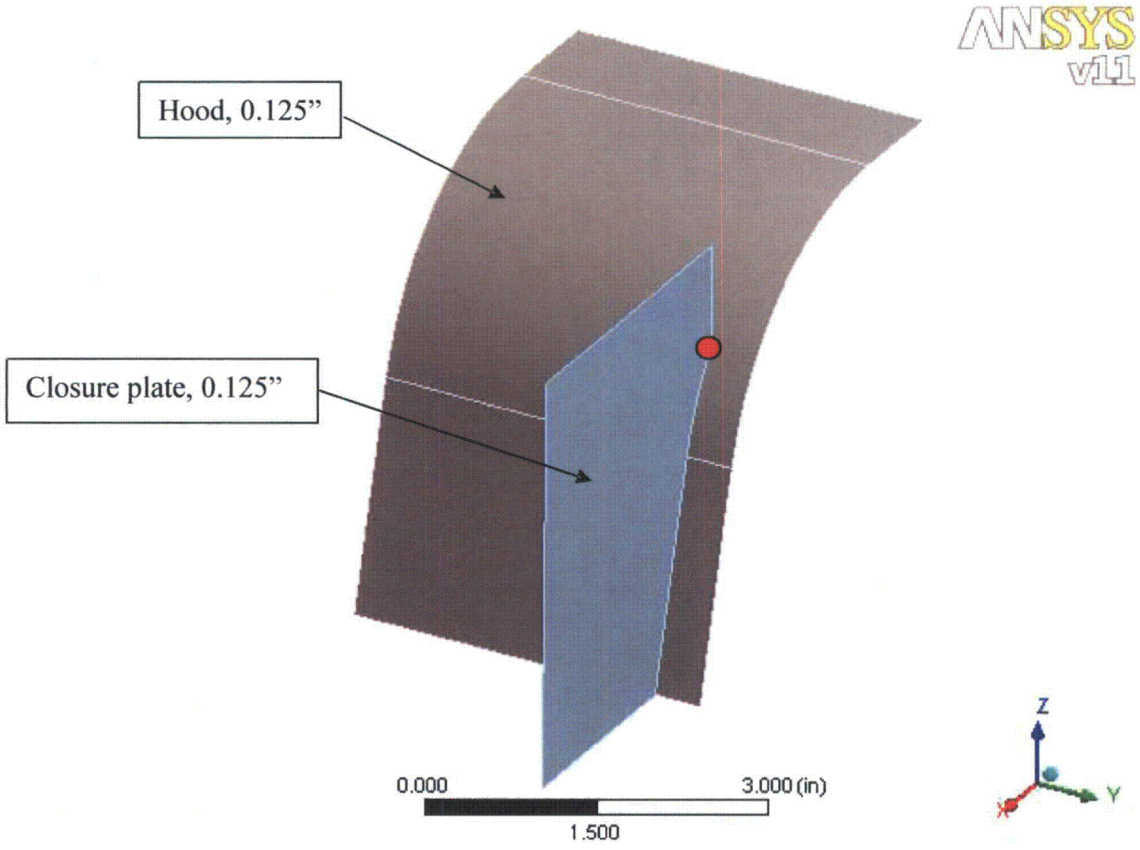

Figure 34a. Shell sub-model node 95172.

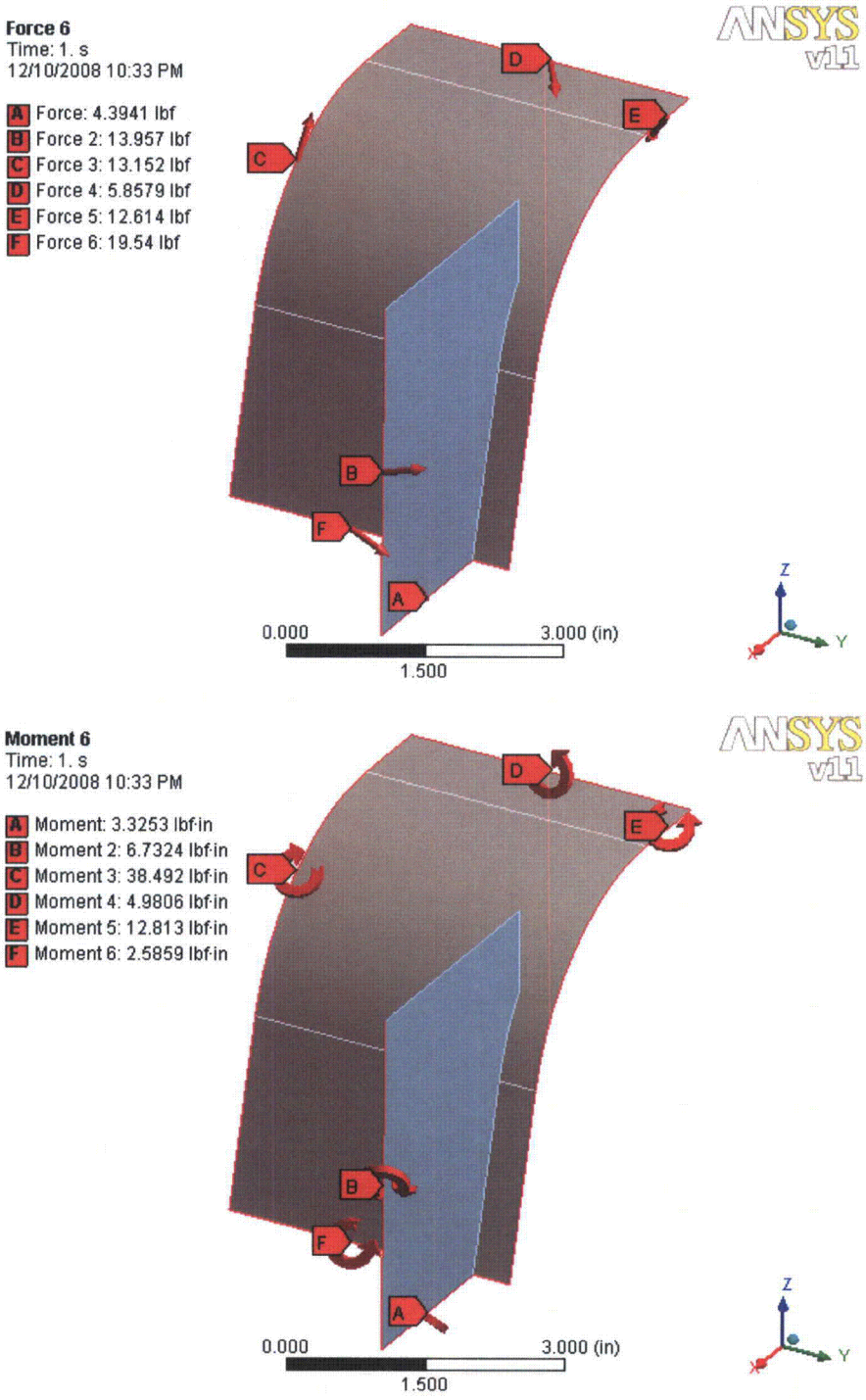

Figure 34b. Forces and moments.

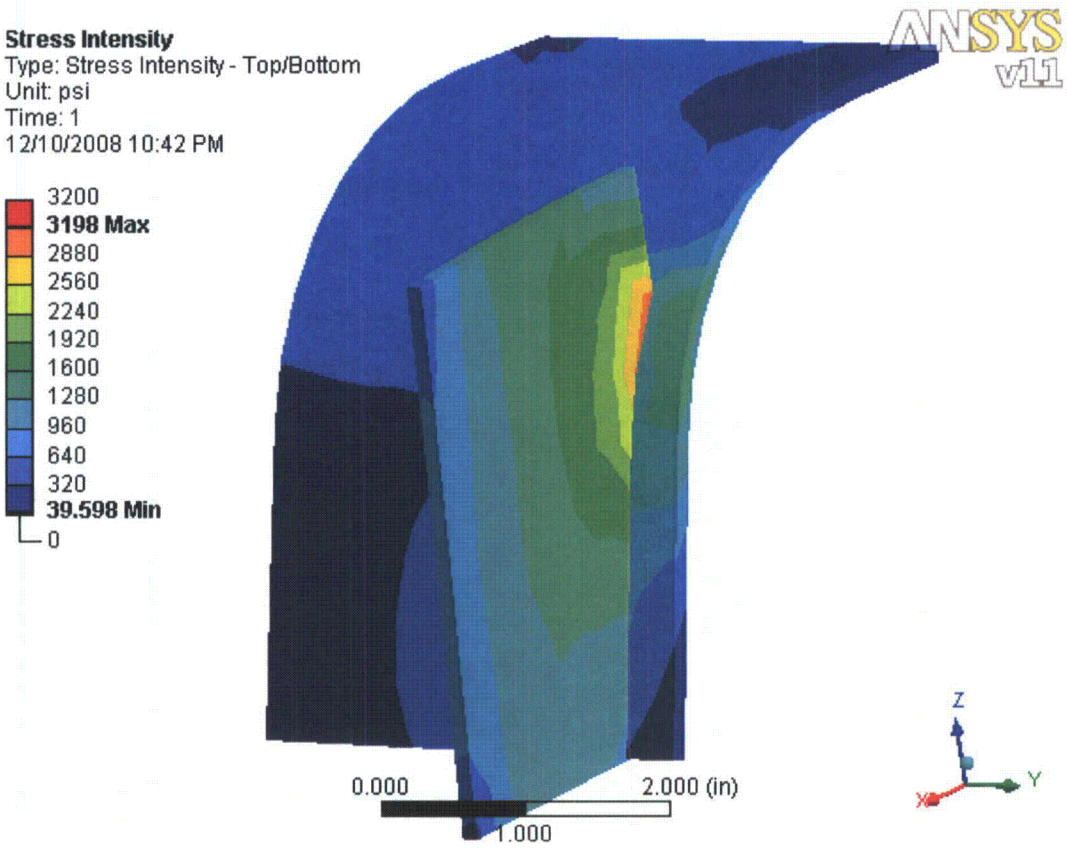

Figure 34c. Shell sub-model stress contours. Stress intensity: 3198 psi.

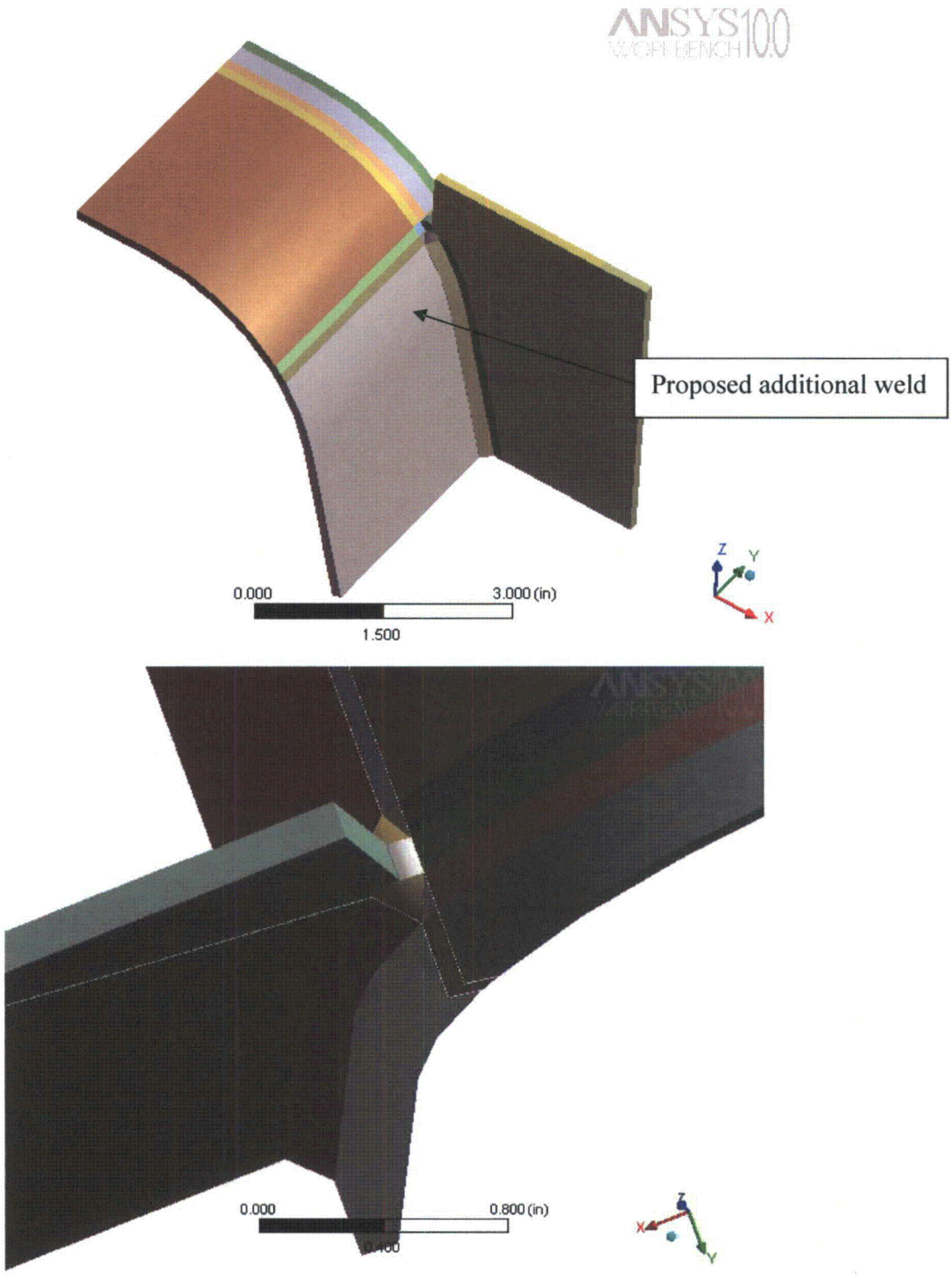

Figure 35a. Solid model geometry.

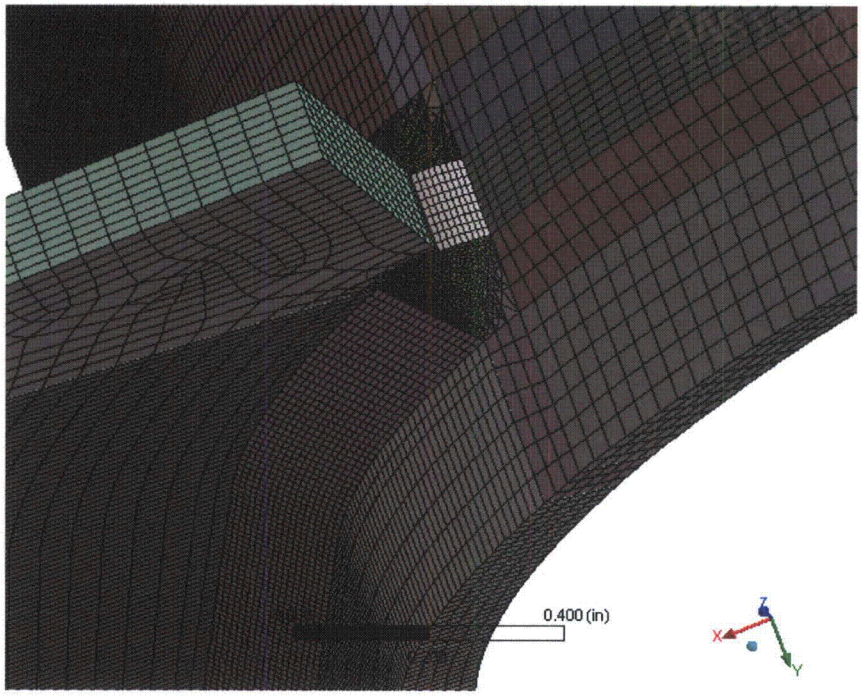

Figure 35b. Solid mesh.

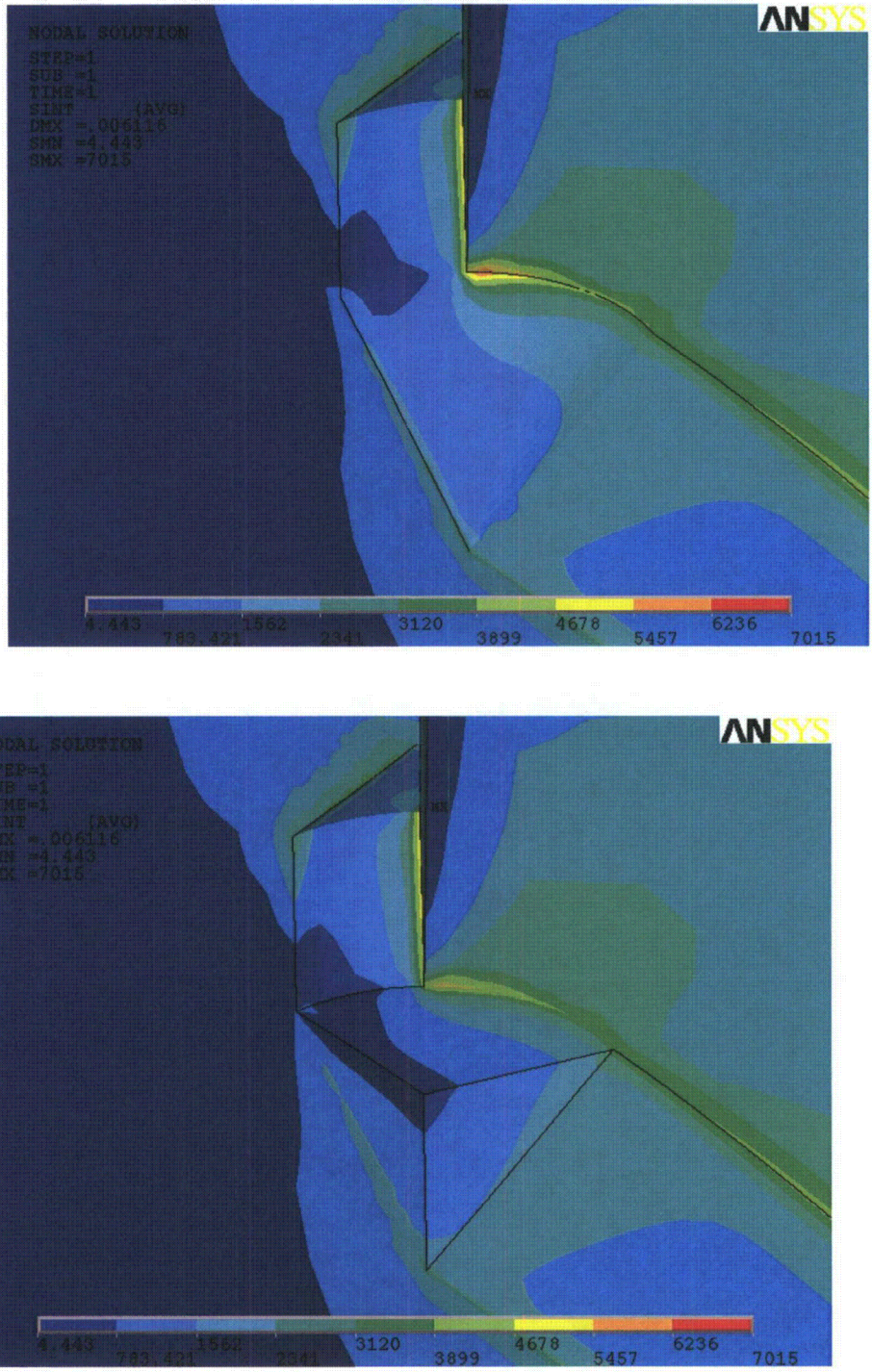

Figure 35c. Stress intensity contours (total) in solid sub-model.

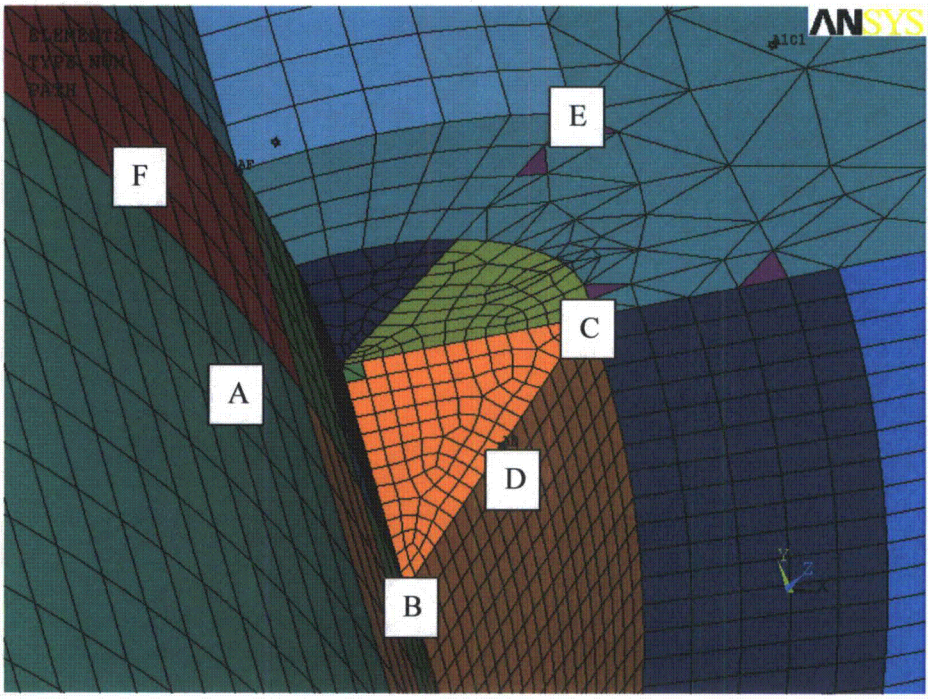

Figure 36a. Linearization paths at the original weld for sub-model node 95172.

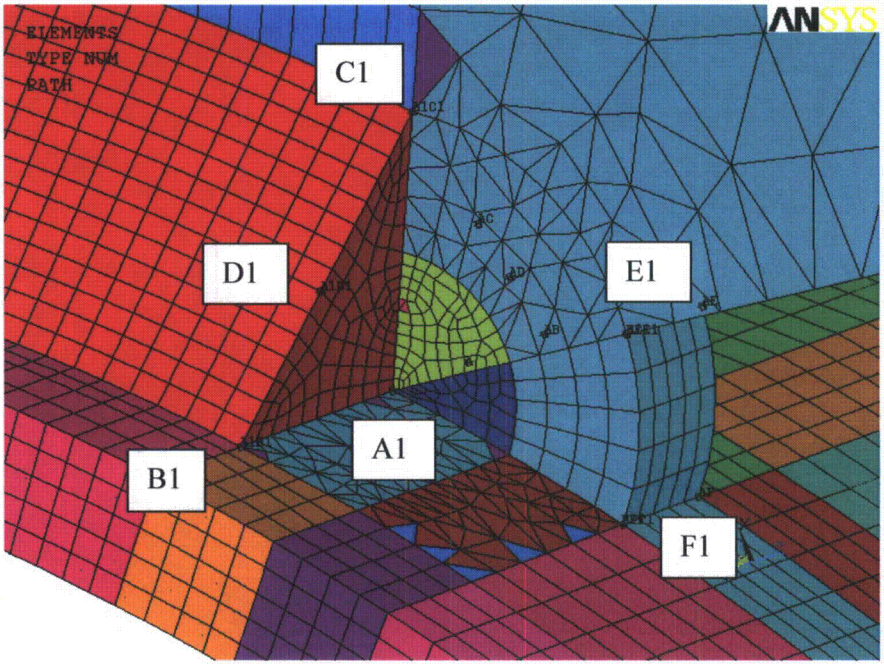

Figure 36b. Linearization paths at the additional weld for sub-model node 95172.

Table 18. Linearized stresses along the linearization paths shown in Figure 36.

Path	Membrane + bending linearized stress intensity, psi
AB	1910
AC	2437
AD	1696
AE	2421
AF	639
A1-B1	2002
A1-C1	2689
A1-D1	1837
A1-E1	2696
A1-F1	1598
C-C1	2762

Sub model node 100327.

The final sub-model involving the closure plate is for a node on the vertical weld connecting the closure plate to the vane bank. It is located 13.5 inches below the top of the weld. The shell element-based sub-model is shown in Figure 37a and involves four components. The extracted forces are shown in Figure 37b and the shell sub-model stress distribution is shown in Figure 37c with a maximum stress intensity stress at the location of 2744 psi. The solid sub-model, mesh and stresses are shown in Figure 38 and, the stress intensity linearization paths depicted in Figure 39. The extracted linearized stresses are tabulated in Table 19 and show a limiting linearized stress in the solid sub-model of **2406 psi**. The stress reduction factor is 2406/2744 = **0.88**.

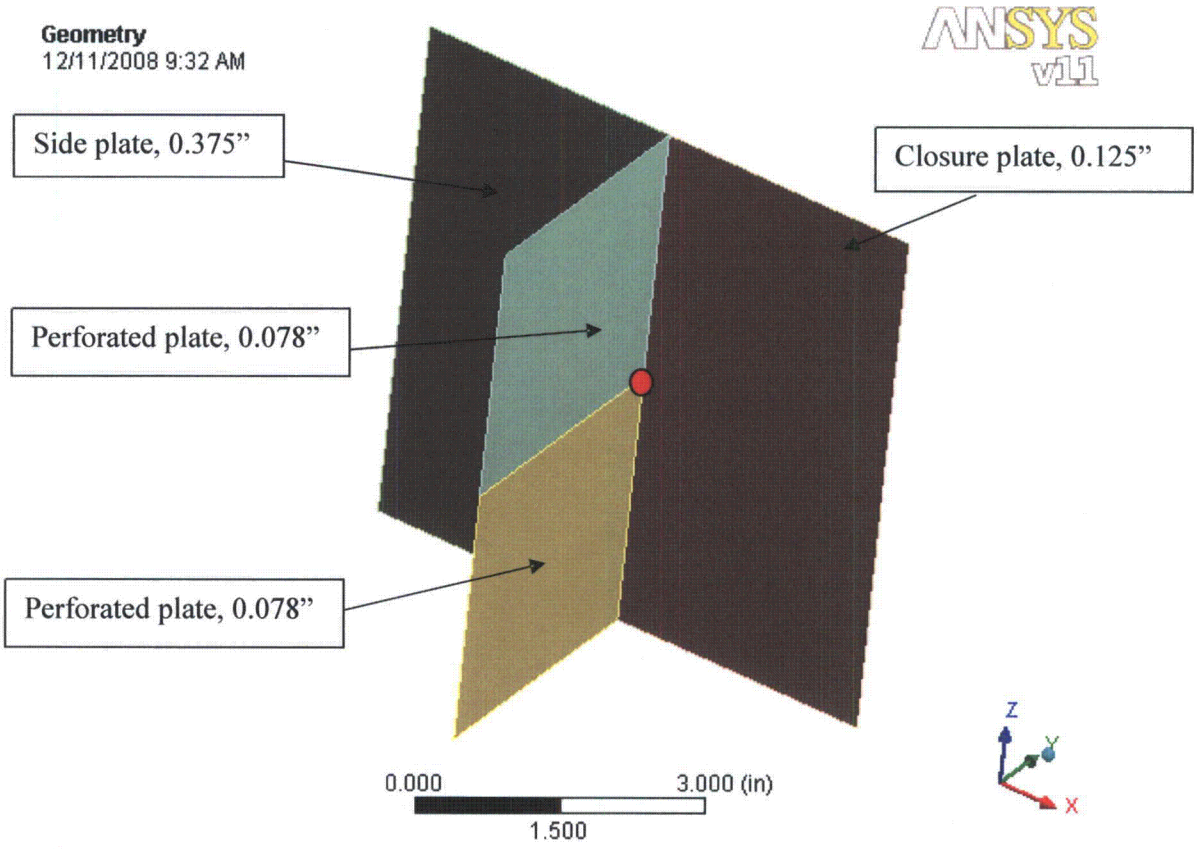

Figure 37a. Shell sub-model node 100327.

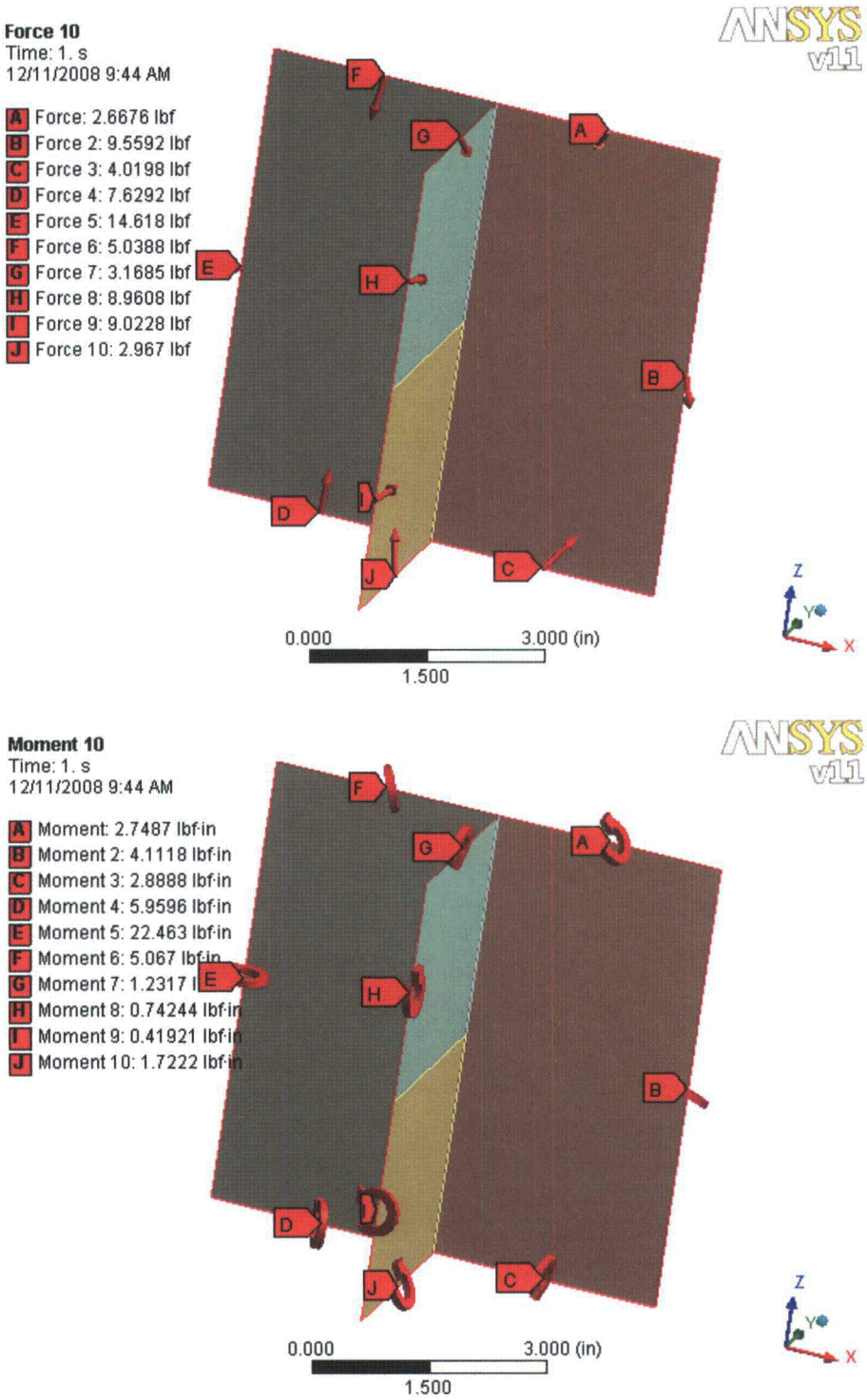

Figure 37b. Forces and moments.

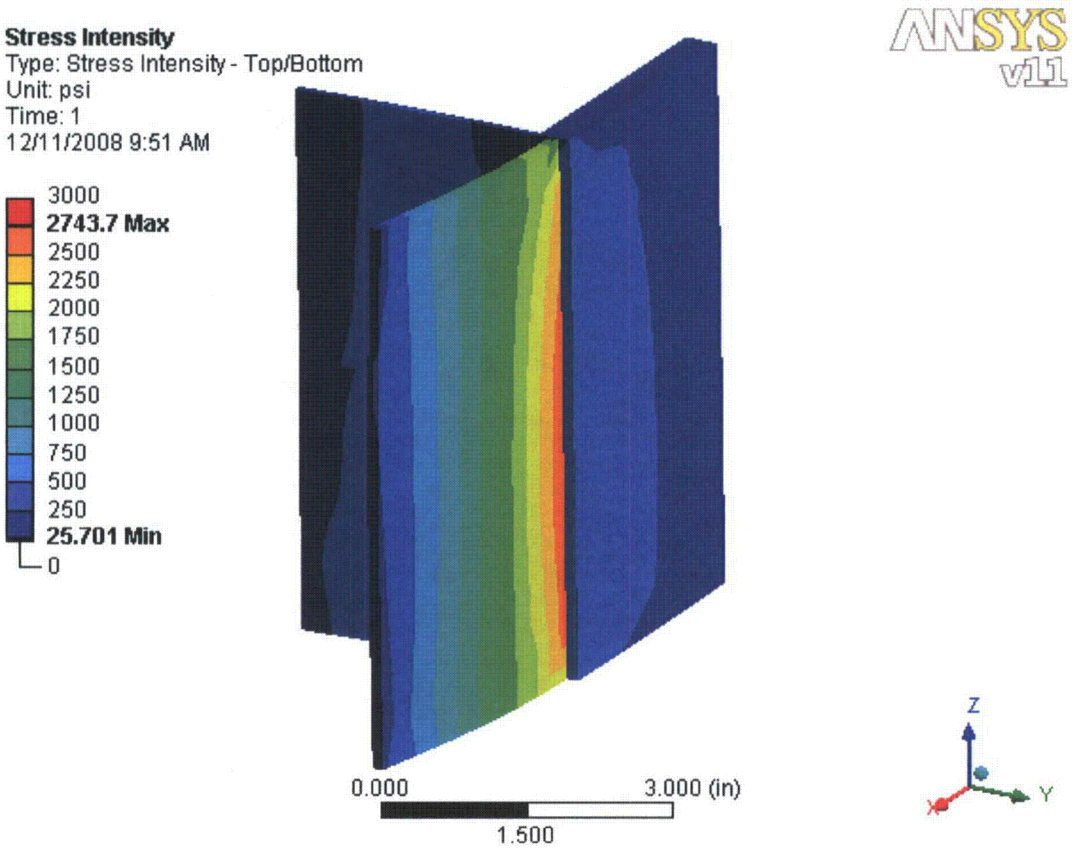

Figure 37c. Shell sub-model stress contours. Stress intensity: 2744 psi.

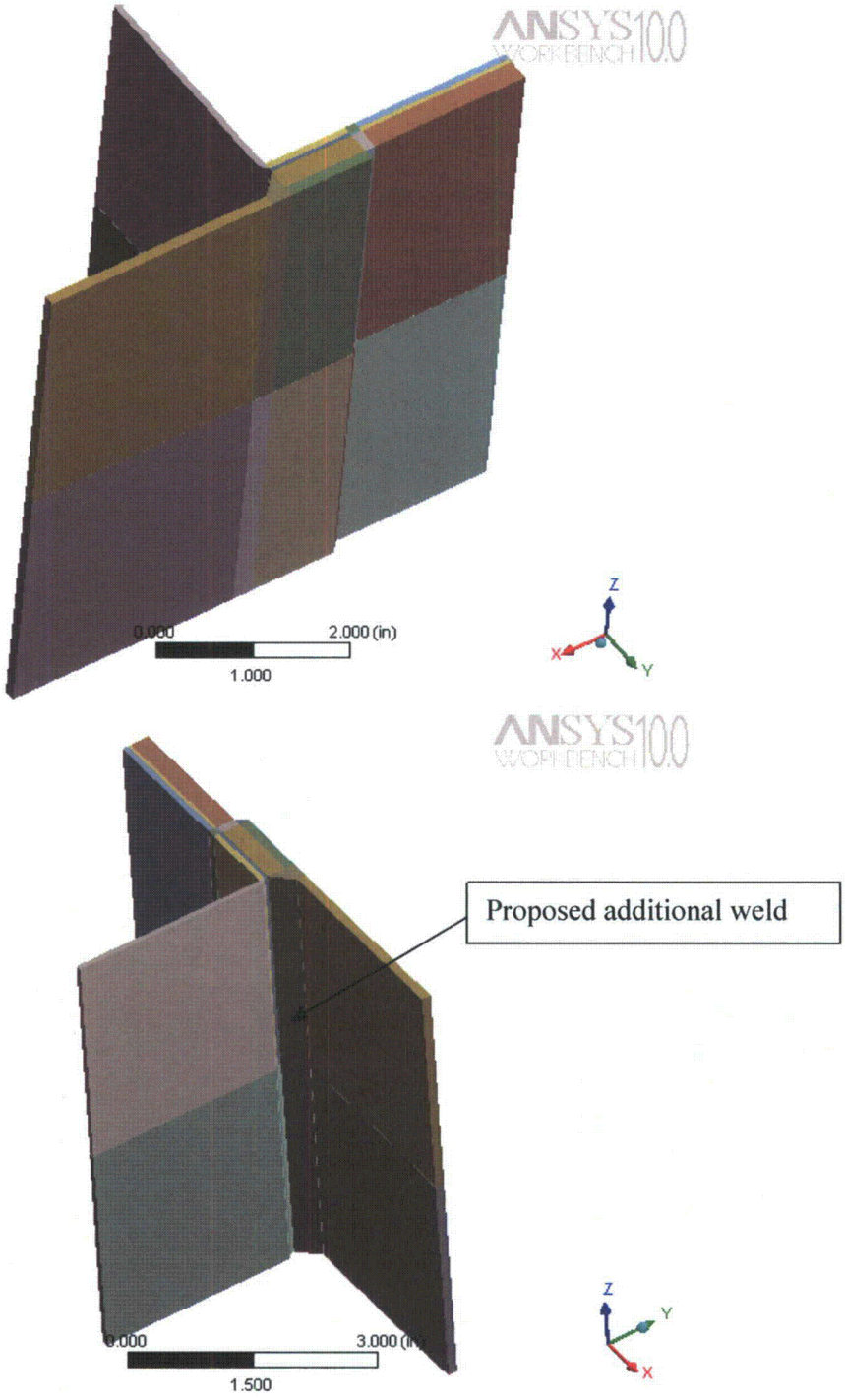

Figure 38a. Solid model geometry.

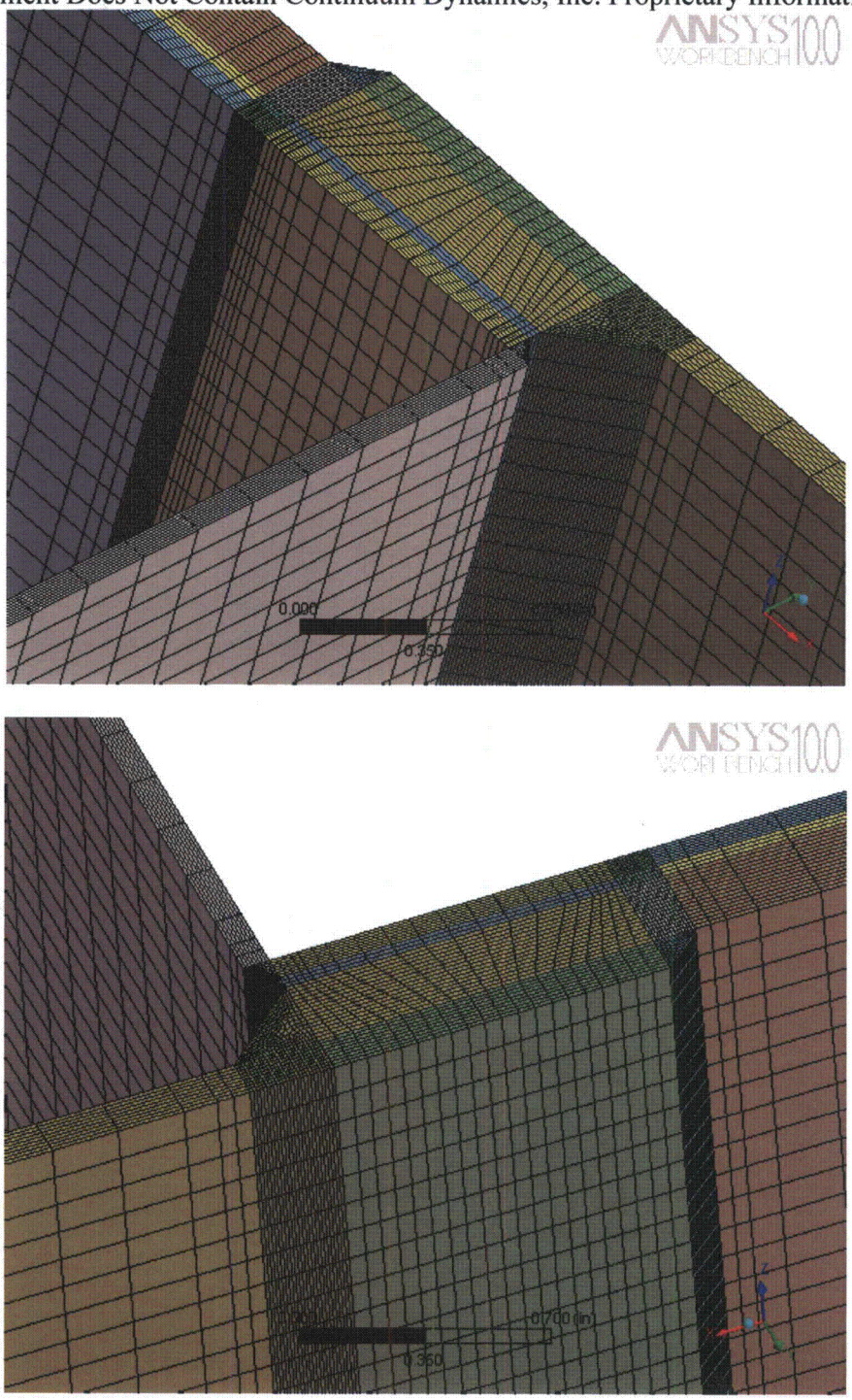

Figure 38b. Solid mesh. Mesh parameters: 567369 nodes, 133680 elements.

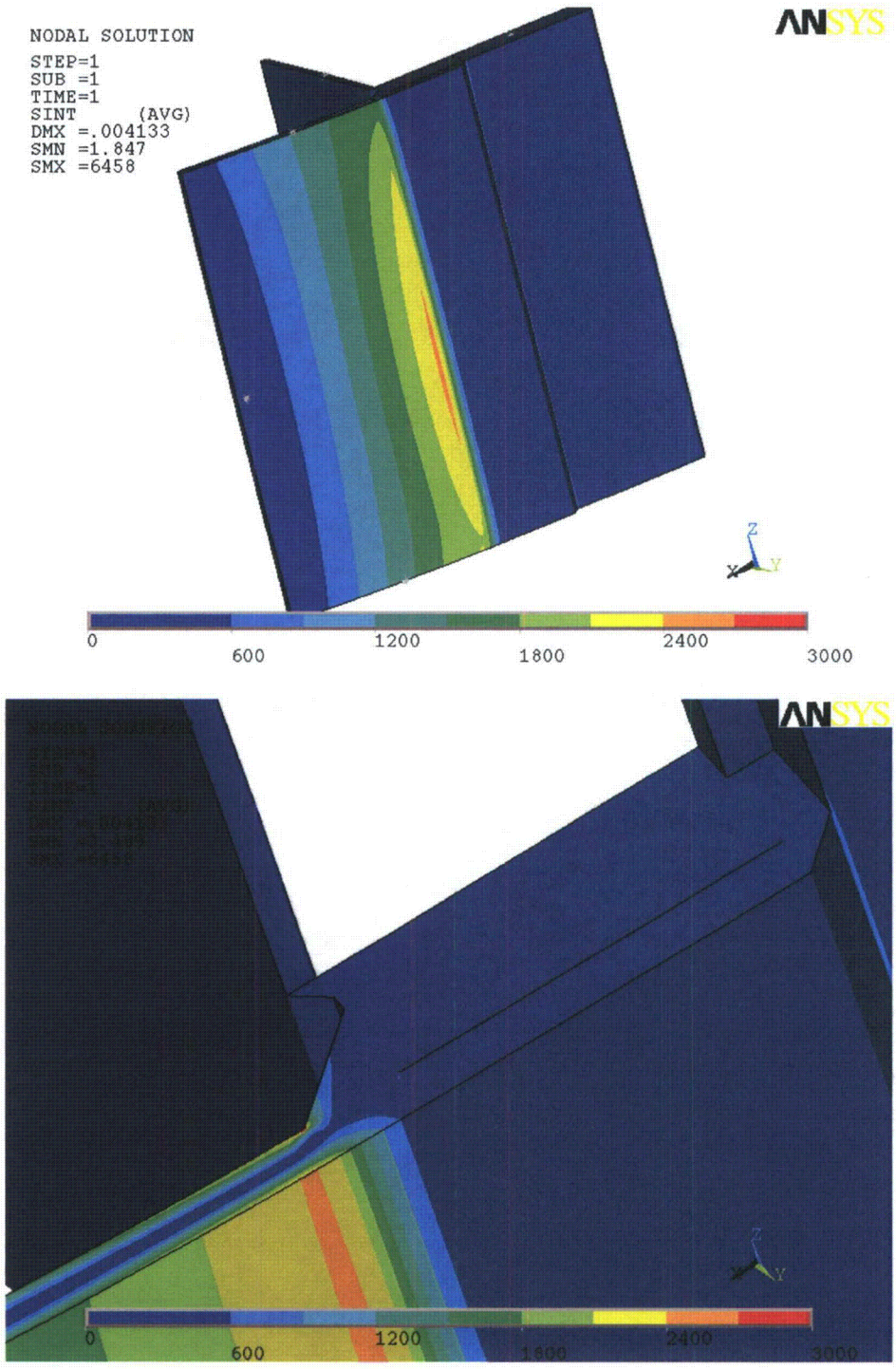

Figure 38c. Stress intensity contours (total) in solid sub-model. Parts of the structure removed to show internal stress distribution (bottom).

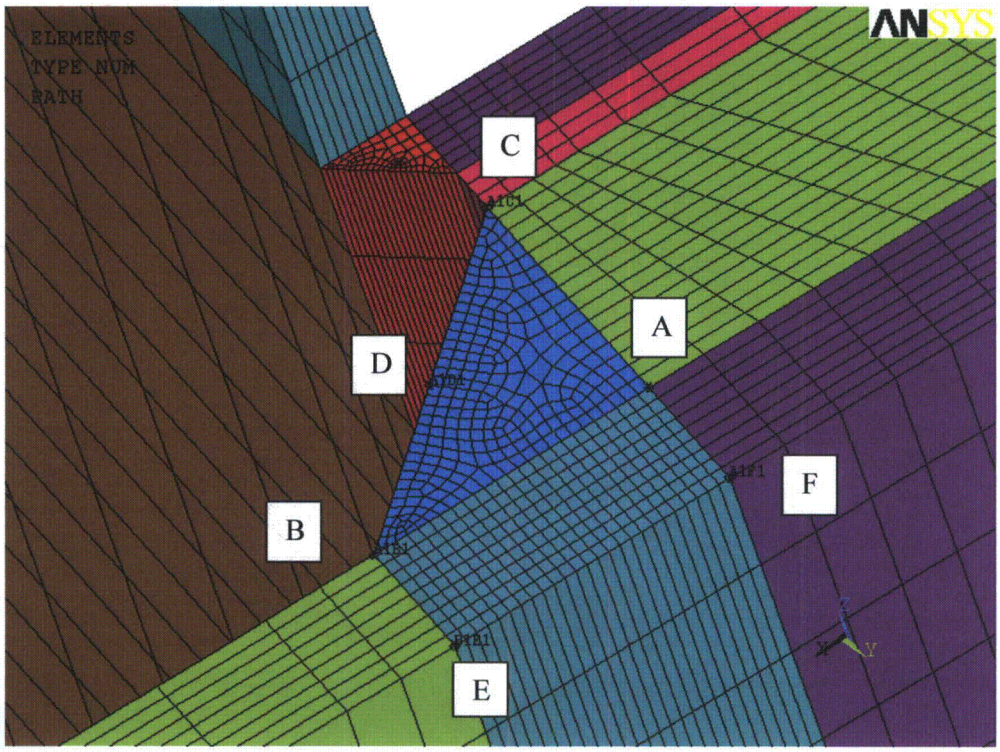

Figure 39. Linearization paths at the additional weld for sub-model node 100327.

Table 19. Linearized stresses along the linearization paths shown in Figure 39.

Path	Membrane + bending linearized stress intensity, psi
AB	1589
AC	439
AD	724
BE	2406
AF	488

Appendix B. Scoping Evaluation of Hood Support Cutout to Alleviate Stress in the Hood/Hood Support/Base Plate Weld

High stresses are found in the global model at the location of the hood support and the outer hood bottom junction, 3263 psi (node 95267 – note that this value is prior to the 1.4/1.8 scaling to account for the full penetration weld factor and which is applied to obtain the results in Table 9). A cut-out is considered to relieve the stress concentration and re-distribute stresses in more favorable manner. The location of the cut-out is chosen to be 0.5" away from the "hot-spot" with a diameter of the cut-out 1.5" (i.e. the center of the cut-out is 1.25" away from the "hot spot"). To estimate the influence of the cut-out the global loading, refined to match stresses at three neighboring locations, was applied to solid element submodels with and without the cut-out. Stress intensity contours for the model with and without the cut-out are shown in Figure 40. The largest linearized stress in the model without the cut-out is found to be 3,403 psi which is a close match to the global value. With the cut-out included the largest linearized stress at the end of the weld using the paths shown in Figure 41 is established as 2,225 psi, which corresponds to a reduction factor of 2225/3403=**0.65**.

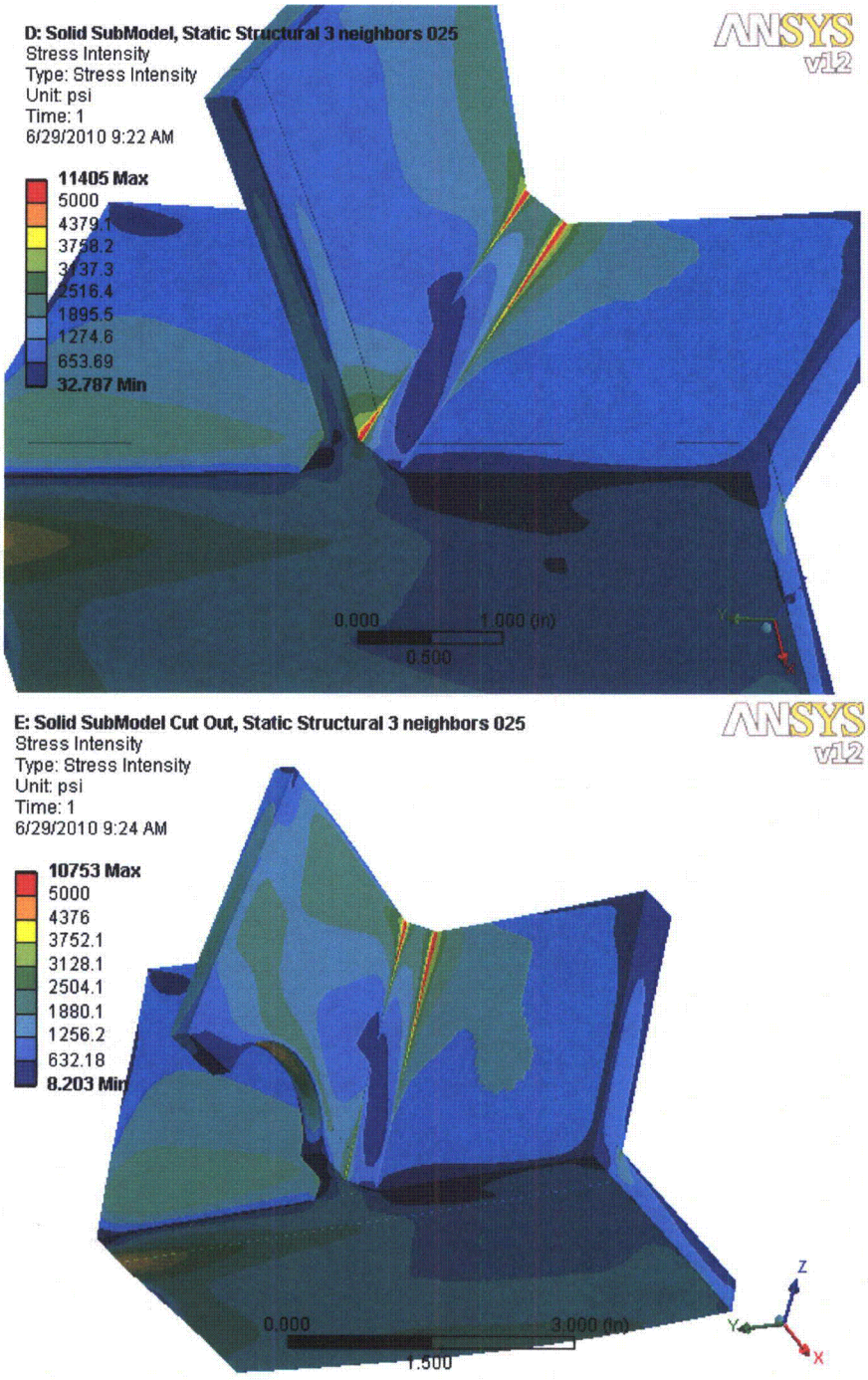

Figure 40. Stress intensity contours with and without cut-out in the solid submodel.

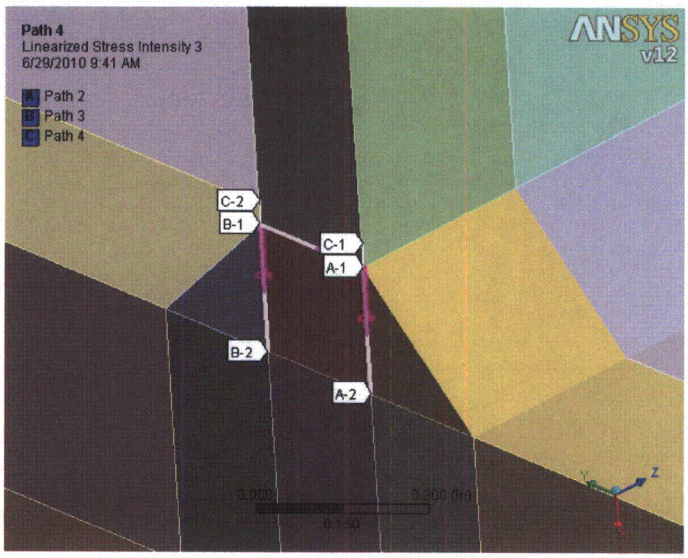

Figure 41. Stress linearization paths A1-A2, B1-B2, C1-C2.